A Non-orthogonal Uplink/Downlink IoT Solution for Next-generation ISAC Systems

Meng Liu, *Student Member, IEEE,* Minglei Yang, *Member, IEEE,* Fa Wei, Huifang Li, Zhaoming Zhang, Arumugam Nallanathan, *Fellow, IEEE* and Lajos Hanzo, *Life Fellow, IEEE*

***Abstract*—An integrated sensing and communication (ISAC) system is investigated, where the base station (BS) provides both uplink and downlink Internet-of-Things (IoT) services as well as target sensing services. Furthermore, non-orthogonal transmission (NO-T) is introduced for improving the spectrum efficiency. The deleterious effects of hardware impairments, channel estimation errors, and imperfect successive interference cancellation are taken into account. Both the exact and asymptotic outage probabilities (OPs) of the IoT devices as well as the probability of successful detection (PoD) are derived for characterizing the communication and sensing (C&S) performances. As a further development, in the presence of the sensing requirements, a communication-centric power allocation (PA) problem is formulated for maximizing the sum rate of the IoT devices. Given the non-convexity of the problem, an alternating optimization algorithm is developed for finding a near-optimal PA. The simulation results confirm the accuracy of the analysis and demonstrate that: (1) The above non-ideal factors degrade the C&S performances; (2) The NO-T ISAC system considered outperforms pure ISAC in terms of both its OP and PoD; (3) Compared to other baseline PA schemes, the proposed algorithm maximizes the sum rates while meeting the sensing requirements.**

***Index Terms*—Integrated sensing and communication, non-orthogonal transmission, performance analysis, power allocation.**

I. Introduction

At the time of writing, the fifth-generation (5G) has been commercialized, hence researchers have turned their attention to the sixth-generation (6G) concepts [1]. At the same time, smart transportation, remote health and the smart home impose demanding technical requirements on the emerging 6G concepts, which include the ingenious combination of communication and sensing (C&S) [2]. It is conjectured that the access density of the 6G Internet-of-Things (IoT) devices will further escalate along with the peak data rate [3], potentially leading to a spectrum crunch, exacerbated by C&S. This problem might be mitigated by sensing-communication coexistence (SCC) and by integrated sensing and communication (ISAC) [4], [5]. Indeed, in the SCC concept, the C&S subsystems operate in the same frequency band independently, but encountering their cross-interference is inevitable [6]. By contrast, the ISAC system utilizes unified hardware resources simultaneously carrying out C&S functions, which significantly mitigates the hardware expenditure [7].

However, traditional orthogonal transmission often leaves the IoT base station (BS) overwhelmed. As a remedy, non-orthogonal transmission (NO-T) may be harnessed for serving multiple IoT devices within the same time/frequency/code domain resource slot [8], [9]. With extensive attention and support from the industry and academia, NO-T may be expected to remain on the center-stage for next-generation IoT systems [10]–[12]. Specifically, superposition coding and successive interference cancellation (SIC) are routinely adopted at the transmitters (TXs) and receivers (RXs) respectively, so that the congested spectrum resources can be effectively exploited [13]. Additionally, in the ISAC hardware integrating TX and RX, NO-T can readily reduce the loop self-interference (LSI) associated with multiple transmission of signals for the IoT devices at the same time compared to the traditional orthogonal transmission [14], [15].

A. Related works

Against the above background, the authors of [16] proposed a non-orthogonal downlink transmission (NO-DLT) assisted ISAC system in which mixed multi-purpose unicast and multicast signals were transmitted for simultaneously serving multiple IoT devices. In [17], based on the premise of meeting the minimum requirements for communication rate and sensing power, a power allocation (PA) algorithm was designed for NO-DLT ISAC systems to maximize the weighted sum of the communication rate and sensing power in the target direction. Furthermore, the C&S performance of the non-orthogonal uplink transmission (NO-ULT) in an ISAC system was analyzed in [18] explicitly, the authors derived the expressions of outage probability (OP) and ergodic sum rate for the communication users as well as the sensing rate for the radar signals. The impact of SIC on the outage and sensing rate performances of ISAC NO-ULT system was investigated in [19]. As a further advance, a cooperative NO-DLT ISAC system was proposed in [20], where the BS communicated with multiple users and simultaneously served as a relay to assist the radar in target

M. Liu, M. Yang, F. Wei, and Z. Zhang are with the National Key Laboratory of Radar Signal Processing, Xidian University, Xi'an, Shaanxi 710071, China (e-mail: liumeng2021@163.com; mlyang@xidian.edu.cn; fwei1220@163.com; zmzhang_sx@163.com).

H. Li is with State Key Laboratory of Integrated Services Networks, Xidian University, Xi'an, Shaanxi 710071, China (e-mail:huifanglixd@gmail.com).

A. Nallanathan is with the School of Electronic Engineering and Computer Science, Queen Mary University of London, London E1 4NS, U.K. (e-mail: a.nallanathan@qmul.ac.uk).

L. Hanzo is with the School of Electronics and Computer Science, University of Southampton, Southampton SO17 1BJ, U.K. (e-mail:lh@ecs.soton.ac.uk).

L. Hanzo would like to acknowledge the financial support of the Engineering and Physical Sciences Research Council projects EP/W016605/1, EP/X01228X/1 and EP/Y026721/1 as well as of the European Research Council's Advanced Fellow Grant QuantCom (Grant No. 789028)

sensing. In [21], a novel macro-micro cooperative system was proposed, in which the micro-station can simultaneously carry out the functions of cooperative relaying and target sensing. More recently, a novel secure NO-DLT ISAC system was developed in [22], where the sensing target was regarded as an eavesdropper. The associated transmit precoding optimization problem was designed for maximizing the sum secrecy rate of the communication users, while meeting both their constraints and the SINR requirements of the echo signal. Indeed, the authors of [16]–[22] demonstrated that the performance of NO-T ISAC systems exceeds that of orthogonal ISAC in the field of both C&S.

To elaborate further, the authors of [4], [6], [13]–[22] focused their research on perfect radio frequency (RF) hardware, even though the RF TXs and RXs suffer from phase noise, in-phase and quadrature-phase imbalance (IQI), and amplifier non-linearities [23], [24]. Furthermore, numerous inexpensive IoT devices are harnessed for reducing the hardware costs, which aggravates the hardware impairments (HIs). As a remedy, advanced compensation algorithms were proposed in [25] to mitigate the influence of HIs, but the residual HIs (RHIs) cannot be neglected [26]. Specifically, the lower bound for the probability of successful detection (PoD) in a full-duplex (FD) SCC system was maximized under the quality of service constraint of the communication users by considering realistic RHIs [27]. As a further advance, optimal PA schemes were designed in [28] for mitigating the mean square error and improve the robustness of a FD SCC system suffering from RHIs. The authors of [29] developed the performance bounds of C&S for an ISAC system according to the peak sidelobe level of radar and the signal-to-interference-plus-noise ratio (SINR) of communication users, where the TX RHIs were taken into account. The effect of RHIs on a cooperative NO-DLT satellite system was studied by deriving both the exact and asymptotic secrecy outage probability (SOP) expressions in [30].

Coincidentally, apart from the RHIs, channel estimation errors (CEEs) also constitute a non-negligible factor in practical systems [31]. As a matter of fact, due to the limited signal feedback, owing to the real-time mobility of the IoT devices, the channel variations between the BS and IoT devices, and the limited coherence time, it is unrealistic to acquire the exact channel state information (CSI) [32]. On this basis, the authors of [28] modeled the CEEs by employing a linear minimum mean square error (LMMSE) estimator. The security of ISAC systems in the presence of realistic CEEs was studied in [33] and [34], where the sensed non-cooperative point-like target was considered to be a malicious eavesdropper. It was shown that the CEEs degraded the C&S performance. The authors of [35] devised a PA scheme for maximizing the sum throughput of the uplink (UL) and downlink (DL) users, where realistic CEEs were considered. Given that vehicular movement degrades the reliability of the communication links and inflicts CEEs, the authors of [36] studied the associated resource allocation issues with the objective of improving the heterogeneous NO-DLT vehicular system throughput.

In a nutshell, previous research [4], [7], [16]–[18], [20]–[22], [29], [33], and [34] laid down the foundations for ISAC systems. Although the performance of FD NO-DLT ISAC systems has been studied in our previous work [21], it is worth emphasizing that UL IoT devices also play a pivotal role in practical communication scenarios. Explicitly the UL-to-DL co-channel interference (CCI) cannot be ignored. Furthermore, to the best of our knowledge, the joint effects of RHIs and CEEs on NO-T ISAC systems have not been documented in the context of ISAC systems that support both the UL and DL actions of IoT devices. As a further practical consideration, realistic RHIs and CEEs imperfections are considered in the context of IoT networks. For example, the ISAC BS provides communication services for both UL and DL IoT devices, as well as simultaneously sense passing pedestrians or vehicles at a traffic light or intersection. Additionally, a PA problem is formulated and served for enhancing the communication performance of the IoT devices. Concretely, the C&S performance of FD NO-T ISAC system are analyzed in the presence of RHIs and CEEs. More particularly, due to the fluctuation of the RHIs and CEEs, it is challenging to implement perfect SIC (pSIC) in NO-T systems. For instance, the authors of [37] studied the performance of a cooperative NO-DLT system in the presence of IQI and imperfect SIC (ipSIC). They pointed out that ipSIC results in avalanche-like error propagation, especially in the face of RHIs. In [38], both the pairwise error probability and bit error rate expressions of the users were derived for characterizing a NO-DLT system, where realistic RHIs and ipSIC were taken into account. The OP and effective capacity of the NO-ULT users in the presence of RHIs and ipSIC were examined in [39] to appraise the system performance attained. Furthermore, the effects of CEEs, ipSIC, and TX RHIs on a cooperative NO-DLT system communicating over $\alpha - \mu$ channels were analyzed in [40]. The contributions [37]–[40] also demonstrated that the ipSIC effects are further exacerbated due to the existence of RHIs.

B. Motivation and Contribution

Motivated by the above parallel, we study an ISAC system in the presence of RHIs, CEEs, and ipSIC, where the BS provides communications services for both the UL and DL of IoT devices, while simultaneously sensing a non-cooperative target. As a further contribution, the resource efficiency can be substantially improved by introducing the FD NO-T concept into ISAC systems. We emphasize that our theoretical analysis quantifies the joint effects of RHIs, CEEs, and ipSIC on the C&S performances of ISAC systems. In addition, the consideration of realistic practical impairments paves the way for hardware design. It is challenging but interesting to conceive solutions for mitigating these non-ideal factors, which will serve as a future study for us. To further clarify the contribution of this paper, a bold comparison between the proposed system and previous concepts is provided in Table I. The explicit contributions of this paper are listed as follows:

- We derive the exact OPs of the UL IoT TXs and DL IoT RXs to evaluate the communication performance of the FD NO-T ISAC system considered. To shed further light on the outage performance, the asymptotic OPs encountered in the high signal-to-noise ratio (SNR) regime

TABLE I: Comparison of contributions between the proposed and other papers

Paper	[4]	[6]	[14]	[15]–[17]	[18]	[20]	[21]	[29]	[33]	[34]	Proposed
SCC	✓	✓									
ISAC	✓		✓	✓	✓	✓	✓	✓	✓	✓	✓
UL			✓			✓					✓
DL	✓	✓		✓	✓		✓	✓	✓	✓	✓
NO-T			✓	✓	✓	✓	✓				✓
PA	✓		✓	✓	✓		✓	✓	✓	✓	✓
Analysis						✓	✓				✓
RHIs								✓			✓
CEEs									✓		✓
FD							✓				✓
CCI											✓
ipSIC											✓

are investigated as well. The results obtained demonstrate that all the RHIs, CEEs, and ipSIC degrade the outage performance of the IoT devices.

- The PoD of the BS and the receiver's operating characteristics (ROC) are derived for characterizing the sensing performance of the FD NO-T ISAC system considered. The results indicate that the introduction of NO-T into ISAC systems boosts the sensing performance of the system considered.
- Finally, a communication-centric design (CCD) PA problem is formulated for further consolidating the system performance and enrich the resource utilization. Concretely, an alternating optimization algorithm is proposed for maximizing the sum rate of the IoT devices subject to the constraint of meeting the sensing requirements by jointly regulating the transmit power of the UL IoT TXs and BS. The simulation results confirm the convergence of the algorithm proposed.

C. Organization and Notations

The remainder of this paper is organized as follows. Section II develops the model of our FD NO-T ISAC system supporting both the UL and DL of IoT devices. Both the exact and asymptotic OPs of the UL and DL of IoT devices are derived in Section III. In Section IV, the sensing capability of the BS is analyzed. A communication-centric PA scheme is formulated in Section V, while Section VI presents some numerical results followed by our conclusions in Section VII.

Notations: In this paper, we use $\mathbb{E}[\cdot]$ to denote the expectation operation, $\mathcal{CN}(a,b)$ represents a complex Gaussian random variable with mean a and variance b, $f_X(\cdot)$ and $F_X(\cdot)$ stand for the probability density function (PDF) and cumulative distribution function (CDF) of X, respectively.

II. System Model

As shown in Fig. 1, we consider a FD NO-T ISAC system, which comprises a FD BS S, a pair of DL IoT devices D_f and D_n, and two UL IoT devices U_f and U_n.[1] Concretely,

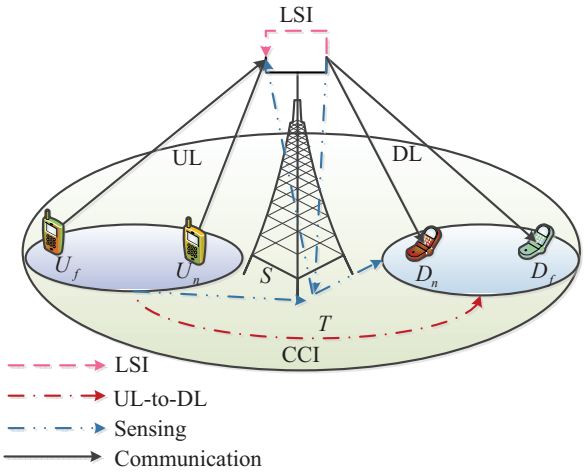

Fig. 1: An illustration of FD NO-T ISAC system.

the UL IoT devices transmit their signals to the BS, while the BS communicates with the DL IoT devices and senses the target simultaneously. It is assumed that all the IoT devices are equipped with a single antenna, while the BS has two antennas, one for transmitting and the other for receiving signals[2]. We adopt $\tilde{h}_{SU_f}$ and $\tilde{h}_{SU_n}$ to denote the estimated UL channels of the $U_f \to S$ and $U_n \to S$ links, respectively. Furthermore, $\tilde{h}_{SD_f}$ and $\tilde{h}_{SD_n}$ denote the estimated DL $S \to D_f$ and $S \to D_n$ channels, respectively. The variable h_{LI} denotes the LSI channel associated with the BS simultaneously transmitting and receiving signals, while $\tilde{h}_{ST}$ and $\tilde{h}_{TS}$ are the estimated sensing channels between the BS and target. Additionally, $\tilde{h}_{ff}$, $\tilde{h}_{fn}$, $\tilde{h}_{nf}$, and $\tilde{h}_{nn}$ represent the estimated UL-to-DL CCI channels of the $U_f \to D_f$, $U_f \to D_n$, $U_n \to D_f$, and $U_n \to D_n$ links, respectively. In practical scenarios, it is challenging to obtain the exact CSI due to the presence of estimation and feedback errors. To this end, the actual channel coefficients can be modeled by employing the LMMSE as $h_i = \tilde{h}_i + e_i, i \in \{SU_f, SU_n, SD_f, SD_n, ST, TS, ff, fn, nf, nn\}$ [28], where $e_i \sim \mathcal{CN}\left(0, \sigma_i^2\right)$ denotes the CEEs, which is independent of $\tilde{h}_i$. For the operation of the system considered, the following

[1]It should be pointed out that the IoT network considered relies on cellular networks. Hence, the IoT devices may indeed be viewed as cellular users, but also as smart and sophisticated IoT video devices, such as tablets, wearables, and so on. Non-cellular IoT systems such as, ZigBee, Bluetooth, Wi-Fi and other IoT networks are beyond the scope of our paper.

[2]As a novel exploration, our focus is on investigating the deleterious effects of RHIs and CEEs on the C&S performance of the NO-T ISAC system, where single-antenna IoT devices and twin-antenna BSs are considered. However, our work may be readily extended to multi-antenna systems, which will be set aside for our future work.

assumptions are stipulated: 1) The signals transmitted form the BS have both C&S functions [4]; 2) The sensing links of UL-target-DL are omitted due to the reflection paths of the signals as well as owing to the low transmit power of the UL IoT devices [35]; 3) The estimated channels are subject to Rayleigh distribution[3].

A. Downlink Transmission

The BS transmits the DL signal $y_S = \sqrt{a_f P_S} x_f + \sqrt{a_n P_S} x_n$ to the RXs and these signals are also used for target sensing, where a_f, a_n, and P_S respectively denote the PA coefficients and transmit power of the BS associated with $a_f + a_n = 1$ and $a_f > a_n$ [41]. Furthermore, x_f and x_n are the expected signals of D_f and D_n, having $\mathbb{E}\left[|x_f|^2\right] = \mathbb{E}\left[|x_n|^2\right] = 1$, respectively. Meanwhile, the DL IoT devices also receive the signals $y_{U_f} = \sqrt{P_{U_f}} s_f$ and $y_{U_n} = \sqrt{P_{U_n}} s_n$ transmitted from the UL IoT devices, where P_{U_f}, P_{U_n}, s_f, and s_n are the transmit power and data symbols of U_f and U_n with $\mathbb{E}\left[|s_f|^2\right] = \mathbb{E}\left[|s_n|^2\right] = 1$, respectively. Therefore, the signal receive at D_f can be expressed as

$$\begin{aligned} y_{D_f} = &\left(h_{SD_f} + w_{D_f}\right)\left(y_S + \eta^t_{SD_f}\right) + h_{ff}\left(y_{U_f} + \eta^t_{ff}\right) \\ &+ h_{nf}\left(y_{U_n} + \eta^t_{nf}\right) + \eta^r_{SD_f} + \eta^r_{ff} + \eta^r_{nf} + n_f, \end{aligned} \tag{1}$$

where $w_{D_f} \sim \mathcal{CN}\left(0, \varpi_{D_f}\right)$ is the interference channel parameter associated with the reflection of the BS's transmit signal to the DL IoT RXs through the target, $n_f \sim \mathcal{CN}\left(0, N_0\right)$ is the additive white Gaussian noise (AWGN) at D_f and N_0 denotes the noise power. Furthermore, we have $\eta^t_{SD_f} \sim \mathcal{CN}\left(0, \kappa^2_{t,S} P_S\right)$, $\eta^t_{ff} \sim \mathcal{CN}\left(0, \kappa^2_{t,U_f} P_{U_f}\right)$, and $\eta^t_{nf} \sim \mathcal{CN}\left(0, \kappa^2_{t,U_n} P_{U_n}\right)$ respectively denote the TXs' RHIs via the links of $S \to D_f$, $U_f \to D_f$ and $U_n \to D_f$, still referring to (1), $\eta^r_{SD_f} \sim \mathcal{CN}\left(0, \kappa^2_{r,D_f} \left|h_{SD_f} + w_{D_f}\right|^2 P_S\right)$, $\eta^r_{ff} \sim \mathcal{CN}\left(0, \kappa^2_{r,D_f} \left|h_{SD_f}\right|^2 P_S\right)$, and $\eta^r_{nf} \sim \mathcal{CN}\left(0, \kappa^2_{r,D_f} |h_{nf}|^2 P_{U_n}\right)$ represent the RXs' RHIs, respectively. More explicitly, $\kappa_{t,S}$, $\kappa_{t,f}$, and $\kappa_{t,n}$ characterize the TXs' impairment levels of S, U_f, and U_n, respectively, and κ_{r,D_f} is the RXs' impairment level of D_f. Based on the previous properties, the receive signal at D_f can be rewritten as

$$\begin{aligned} y_{D_f} = &\underbrace{\left(h_{SD_f} + w_{D_f}\right)\left(y_S + \eta_{SD_f}\right)}_{\text{DL Signal \& RHIs \& CEEs}} \\ &+ \underbrace{h_{ff}\left(y_{U_f} + \eta_{ff}\right) + h_{nf}\left(y_{U_n} + \eta_{nf}\right)}_{\text{CCI \& RHIs \& CEEs}} + n_f, \end{aligned} \tag{2}$$

where $\eta_{SD_f} \sim \mathcal{CN}\left(0, \kappa^2_{SD_f} P_S\right)$, $\eta_{ff} \sim \mathcal{CN}\left(0, \kappa^2_{ff} P_{U_f}\right)$, and $\eta_{nf} \sim \mathcal{CN}\left(0, \kappa^2_{nf} P_{U_n}\right)$ denote the composite RHIs via the links of $S \to D_f$, $U_f \to D_f$ and $U_n \to D_f$, respectively. Furthermore, we can obtain $\kappa_{SD_f} = \sqrt{\kappa^2_{t,S} + \kappa^2_{r,D_f}}$, $\kappa_{ff} = \sqrt{\kappa^2_{t,U_f} + \kappa^2_{r,D_f}}$, and $\kappa_{nf} = \sqrt{\kappa^2_{t,U_n} + \kappa^2_{r,D_f}}$.

Similar to (2), the receive signal at D_n can be expressed as

$$\begin{aligned} y_{D_n} = &\underbrace{\left(h_{SD_n} + w_{D_n}\right)\left(y_S + \eta_{SD_n}\right)}_{\text{DL Signal \& RHIs \& CEEs}} \\ &+ \underbrace{h_{fn}\left(y_{U_f} + \eta_{fn}\right) + h_{nn}\left(y_{U_n} + \eta_{nn}\right)}_{\text{CCI \& RHIs \& CEEs}} + n_n, \end{aligned} \tag{3}$$

where $w_{D_n} \sim \mathcal{CN}\left(0, \varpi_{D_n}\right)$ represents the interference channel parameter of the $S \to T \to D_n$ links, $n_n \sim \mathcal{CN}\left(0, N_0\right)$ denotes the AWGN at D_n, $\eta_{SD_n} \sim \mathcal{CN}\left(0, \kappa^2_{SD_n} P_S\right)$, $\eta_{fn} \sim \mathcal{CN}\left(0, \kappa^2_{fn} P_{U_f}\right)$, and $\eta_{nn} \sim \mathcal{CN}\left(0, \kappa^2_{nn} P_{U_n}\right)$ are the composite RHIs by the links of $S \to D_n$, $U_f \to D_n$, and $U_n \to D_n$, respectively.

According to the NO-DLT protocol, only x_f is decoded at D_f. Specifically, the signal received at D_f can be divided into five parts: (1) The desired signal of D_f, $\tilde{h}_{SD_f}\sqrt{a_f P_S} x_f$; (2) Interference from the desired signal D_n, $\tilde{h}_{SD_f}\sqrt{a_n P_S} x_n$; (3) Interference from the target's reflection, $w_{D_f}\left(y_S + \eta_{SD_f}\right)$; (4) RHIs, CEEs, and CCI, $e_{SD_f}\left(y_S + \eta_{SD_f}\right) + h_{SD_f}\eta_{SD_f} + h_{ff}\left(y_{U_f} + \eta_{ff}\right) + h_{nf}\left(y_{U_n} + \eta_{nf}\right)$; and (5) AWGN. Thus, the receive SINR of x_f at D_f is expressed as

$$\gamma^{x_f}_{D_f} = \frac{a_f \rho_{SD_f} \gamma_S}{\left(H_{SD_f} - a_f \rho_{SD_f}\right)\gamma_S + H_{ff}\gamma_{U_f} + H_{nf}\gamma_{U_n} + 1}, \tag{4}$$

where we have $\gamma_S = P_S/N_0$, $\gamma_{U_f} = P_{U_f}/N_0$, and $\gamma_{U_n} = P_{U_n}/N_0$. Furthermore, we also have

$$\begin{aligned} H_{ff} &= \left(1 + \kappa^2_{ff}\right)\left(\rho_{ff} + \sigma^2_{ff}\right), \\ H_{nf} &= \left(1 + \kappa^2_{nf}\right)\left(\rho_{nf} + \sigma^2_{nf}\right), \\ H_{SD_f} &= \left(1 + \kappa^2_{SD_f}\right)\left(\rho_{SD_f} + \sigma^2_{SD_f} + \varpi_{D_f}\right). \end{aligned}$$

For D_n, the signal received at D_n can be divided into five parts: (1) The desired signal of D_f, $\tilde{h}_{SD_n}\sqrt{a_n P_S} x_n$; (2) Interference by the desired signal D_f, $\tilde{h}_{SD_n}\sqrt{a_f P_S} x_f$; (3) Interference from the target's reflection, $w_{D_n}\left(y_S + \eta_{SD_n}\right)$; (4) RHIs, CEEs, and CCI, $e_{SD_n}\left(y_S + \eta_{SD_n}\right) + h_{SD_n}\eta_{SD_n} + h_{fn}\left(y_{U_f} + \eta_{fn}\right) + h_{nn}\left(y_{U_n} + \eta_{nn}\right)$; and (5) AWGN. Therefore, in view of the ipSIC, the receive SINRs of x_f and x_n at D_n are respectively expressed as

$$\gamma^{x_f}_{D_n} = \frac{a_f \rho_{SD_n} \gamma_S}{\left(H_{SD_n} - a_f \rho_{SD_n}\right)\gamma_S + H_{fn}\gamma_{U_f} + H_{nn}\gamma_{U_n} + 1}, \tag{5}$$

$$\gamma^{x_n}_{D_n} = \frac{a_n \rho_{SD_n} \gamma_S}{\left(H_{SD_n} + \left(\varepsilon a_f - 1\right)\rho_{SD_n}\right)\gamma_S + H_{fn}\gamma_{U_f} + H_{nn}\gamma_{U_n} + 1}, \tag{6}$$

$\varepsilon \in [0, 1]$ represents the ipSIC coefficient. Specifically, $\varepsilon = 0$ and $\varepsilon = 1$ indicate pSIC and no SIC execution at D_n, respectively. Furthermore, we also have

$$\begin{aligned} H_{fn} &= \left(1 + \kappa^2_{fn}\right)\left(\rho_{fn} + \sigma^2_{fn}\right), \\ H_{nn} &= \left(1 + \kappa^2_{nn}\right)\left(\rho_{nn} + \sigma^2_{nn}\right), \\ H_{SD_n} &= \left(1 + \kappa^2_{SD_n}\right)\left(\rho_{SD_n} + \sigma^2_{SD_n} + \varpi_{D_n}\right). \end{aligned}$$

[3]The PDF and CDF of the channel gains $\rho_i = \left|\tilde{h}_i\right|^2, i \in \left\{SU_f, SU_n, SD_f, SD_n, ST, TS, ff, fn, nf, nn\right\}$ are respectively given by $f_{\rho_i}(x) = e^{-x/\beta_i}/\beta_i$ and $F_{\rho_i}(x) = 1 - e^{-x/\beta_i}$, where $\beta_i = h/\sqrt{1 + d_i^{\upsilon}}$ characterizes the channel variance, $h \sim \mathcal{CN}(0, 1)$ denotes the complex channel coefficient, d_i and υ are the distance and path loss exponent between the nodes.

$$y_{\text{BS}} = \underbrace{\left(h_{SU_f} + w_{U_f}\right)\left(y_{U_f} + \eta_{SU_f}\right) + \left(h_{SU_n} + w_{U_n}\right)\left(y_{U_n} + \eta_{SU_n}\right)}_{\text{UL Signal \& RHIs \& CEEs}} + \underbrace{\delta h_{SS}\left(y_S + \eta_{SS}\right)}_{\text{Echo \& RHIs \& CEEs}} + \underbrace{h_{LI} y_S}_{\text{LSI}} + n_S. \tag{7}$$

$$\gamma_{\text{BS}}^{s_f} = \frac{\rho_{SU_f}\gamma_{U_f}}{\left(H_{SU_f} - \rho_{SU_f}\right)\gamma_{U_f} + \left(H_{SU_n} + \varepsilon\rho_{SU_n}\right)\gamma_{U_n} + \left(H_{SS}\delta^2 + \rho_{LI}\right)\gamma_S + 1}. \tag{9}$$

B. Uplink Transmission

As for the UL transmission, U_f and U_n transmit y_{U_f} and y_{U_n} to the BS, respectively. Additionally, the BS receives the echo from the target as well. Therefore, the signal received at the BS can be expressed as (7), shown at the top of the next page, where we have $h_{SS} = \tilde{h}_{SS} + e_{SS}$ with $\tilde{h}_{SS} = \tilde{h}_{ST}\tilde{h}_{TS}$, $w_{U_f} \sim \mathcal{CN}\left(0, \varpi_{U_f}\right)$ and $w_{U_n} \sim \mathcal{CN}\left(0, \varpi_{U_n}\right)$ respectively denote the composite channel parameters of $U_f \to T \to S$ and $U_n \to T \to S$, $n_S \sim \mathcal{CN}\left(0, N_0\right)$ is the AWGN at S. Furthermore, $\eta_{SU_f} \sim \mathcal{CN}\left(0, \kappa_{SU_f}^2 P_{U_f}\right)$, $\eta_{SU_n} \sim \mathcal{CN}\left(0, \kappa_{SU_n}^2 P_{U_n}\right)$, and $\eta_{SS} \sim \mathcal{CN}\left(0, \kappa_{SS}^2 P_S\right)$ represent the composite RHIs via the links of $U_f \to S$, $U_n \to S$, and $S \to T \to S$, respectively. The variable δ represents the scattering coefficient of the target, which is related both to the azimuth and structure of the target and to the wavelength of the transmit signal [42].

As for the NO-ULT, the IoT TXs with poor channels are allocated less transmit power, so that the SIC sensitivity can be reinforced [43], [44]. Therefore, in this paper, we assume that $P_{U_n} > P_{U_f}$. The signal received at the BS can be divided into six parts: (1) The transmit signal of U_f, $\tilde{h}_{SU_f} y_{U_f}$; (2) The transmit signal of U_n, $\tilde{h}_{SU_n} y_{U_n}$; (3) The signal reflected by the target: $w_{U_f}\left(y_{U_f} + \eta_{SU_f}\right) + w_{U_n}\left(y_{U_n} + \eta_{SU_n}\right) + \delta h_{SS}\left(y_S + \eta_{SS}\right)$; (4) RHIs and CEEs, $e_{SU_f}\left(y_{U_f} + \eta_{SU_f}\right) + e_{SU_n}\left(y_{U_n} + \eta_{SU_n}\right)$; (5) LSI, $h_{LI} y_S$; and (6) AWGN. According to the NO-ULT protocol, s_n and s_f are decoded at the BS sequentially by using SIC. Thus, the received SINRs of s_n at the BS can be expressed as

$$\gamma_{\text{BS}}^{s_n} = \frac{\rho_{SU_n}\gamma_{U_n}}{H_{SU_f}\gamma_{U_f} + H_{SU_n}\gamma_{U_n} + H_{SS}\delta^2\gamma_S + \rho_{LI}\gamma_S + 1}. \tag{8}$$

The SINR of s_f received at the BS is given by (9), shown at the top of the next page, where we have

$$\begin{aligned} H_{SS} &= \left(\rho_{SS} + \sigma_{SS}^2\right)\left(1 + \kappa_{SS}^2\right), \\ H_{SU_f} &= \left(\rho_{SU_f} + \sigma_{SU_f}^2 + \varpi_{U_f}\right)\left(1 + \kappa_{SU_f}^2\right), \\ H_{SU_n} &= \kappa_{SU_n}^2 \rho_{SU_n} + \left(1 + \kappa_{SU_n}^2\right)\left(\sigma_{SU_n}^2 + \varpi_{U_n}\right). \end{aligned}$$

Remark 1. *It should be pointed out that although multi-path propagation may improve the communication performance of the IoT devices, for this to happen, the accurate estimation of the channel parameters is required, which is extremely challenging in practical scenarios. Consequently, we assume that the multi-path propagation reduces the SINRs received at S, D_f, and D_n.*

III. Communication Performance

In this section, both the exact and asymptotic OPs of the IoT devices are derived for characterizing the communication performance of our FD NO-T ISAC system in the presence of RHIs, CEEs, and ipSIC.

A. Downlink Transmission

1) OP of D_f: An outage event occurs at D_f, when x_f cannot be decoded at D_f via the $S \to D_f$ link. Thus, the OP of D_f can be expressed as

$$\text{P}_{\text{out,nid}}^{D_f} = \Pr\left(\gamma_{D_f}^{x_f} < \gamma_{\text{thf}}^{\text{DL}}\right), \tag{10}$$

where $\gamma_{\text{thf}}^{\text{DL}}$ denotes the SNR threshold of x_f. The exact OP of D_f is given in the following theorem.

Theorem 1. *The exact OP of D_f is expressed as*

$$\text{P}_{\text{out,nid}}^{D_f} = 1 - \frac{\beta_{SD_f}^2}{\left(V_1\beta_{ff} + \beta_{SD_f}\right)\left(V_2\beta_{nf} + \beta_{SD_f}\right)} e^{-\frac{V_3}{\beta_{SD_f}}}, \tag{11}$$

where we have $V_1 = \left(1 + \kappa_{ff}^2\right)\gamma_{U_f}\theta$, $V_2 = \left(1 + \kappa_{nf}^2\right)\gamma_{U_n}\theta$,

$$\begin{aligned} V_3 &= \Big[\left(1 + \kappa_{SD_f}^2\right)\left(\sigma_{SD_f}^2 + \varpi_{D_f}\right)\gamma_S + \left(1 + \kappa_{ff}^2\right)\sigma_{ff}^2\gamma_{U_f} \\ &\quad + \left(1 + \kappa_{nf}^2\right)\sigma_{nf}^2\gamma_{U_n} + 1\Big]\theta, \\ \theta &= \frac{\gamma_{thf}^{\text{DL}}}{\left[a_f - \left(a_n + \kappa_{SD_f}^2\right)\gamma_{thf}^{DL}\right]\gamma_S}. \end{aligned}$$

Furthermore, we also have $a_f > \left(a_n + \kappa_{SD_f}^2\right)\gamma_{\text{thf}}^{\text{DL}}$, *otherwise* $\text{P}_{\text{out,nid}}^{D_f} = 1$.

Proof. See Appendix A. □

The asymptotic OP of D_f in the high-SNR regime is given in the following corollary.

Corollary 1. *The asymptotic OP of D_f in the high-SNR regime is expressed as*

$$\text{P}_{\text{out,nid}}^{D_f,\infty} = 1 - e^{-\frac{V_3^\infty}{\beta_{SD_f}}}, \tag{12}$$

where V_3^∞ is given by

$$V_3^\infty = \frac{\left(1 + \kappa_{SD_f}^2\right)\left(\sigma_{SD_f}^2 + \varpi_{D_f}\right)\gamma_{\text{thf}}^{\text{DL}}}{a_f - \left(a_n + \kappa_{SD_f}^2\right)\gamma_{\text{thf}}^{\text{DL}}}. \tag{13}$$

Proof. In the high-SNR regime, the received SINR of x_f at D_f is given by

$$\gamma_{D_f}^{x_f,\infty} = \frac{a_f \rho_{SD_f}}{H_{SD_f} - a_f \rho_{SD_f}}. \tag{14}$$

Upon substituting (14) into (10), and using the PDF and CDF of ρ_i, (12) can be obtained after some further mathematical manipulations. □

2) OP of D_n: An outage event occurs at D_n, when either x_f or x_n cannot be decoded successfully at D_n via the $S \to D_n$ link. Thus, the OP of D_n can be expressed as

$$\mathrm{P}_{\text{out,nid}}^{D_n} = 1 - \Pr\left(\gamma_{D_n}^{x_f} > \gamma_{\text{thf}}^{\text{DL}}, \gamma_{D_n}^{x_n} > \gamma_{\text{thn}}^{\text{DL}}\right), \tag{15}$$

where $\gamma_{\text{thn}}^{\text{DL}}$ denotes the SNR threshold of x_n. The exact OP of D_n is given in the following theorem.

Theorem 2. *The exact OP of D_n is expressed as*

$$\mathrm{P}_{\text{out,nid}}^{D_n} = 1 - \frac{\beta_{SD_n}^2}{\left(W_1\beta_{fn} + \beta_{SD_n}\right)\left(W_2\beta_{nn} + \beta_{SD_n}\right)} e^{-\frac{W_3}{\beta_{SD_n}}}, \tag{16}$$

where we have $W_1 = \left(1 + \kappa_{fn}^2\right)\gamma_{U_f}\chi$, $W_2 = \left(1 + \kappa_{nn}^2\right)\gamma_{U_n}\chi$,

$$W_3 = \left[\left(1 + \kappa_{SD_n}^2\right)\left(\sigma_{SD_n}^2 + \varpi_{D_n}\right)\gamma_S + \left(1 + \kappa_{fn}^2\right)\sigma_{fn}^2\gamma_{U_f} + \left(1 + \kappa_{nn}^2\right)\sigma_{nn}^2\gamma_{U_n} + 1\right]\chi.$$

Furthermore, $\chi = \max\left(\chi_1, \chi_2\right)$ *with* $a_f > \left(a_n + \kappa_{SD_n}^2\right)\gamma_{\text{thf}}^{\text{DL}}$ *and* $a_n > \left(\varepsilon a_f + \kappa_{SD_n}^2\right)\gamma_{\text{thn}}^{\text{DL}}$, *otherwise* $\mathrm{P}_{\text{out,nid}}^{D_n} = 1$. χ_1 *and* χ_2 *are respectively given by*

$$\chi_1 = \frac{\gamma_{\text{thf}}^{\text{DL}}}{\left[a_f - \left(a_n + \kappa_{SD_n}^2\right)\gamma_{\text{thf}}^{\text{DL}}\right]\gamma_S},$$
$$\chi_2 = \frac{\gamma_{\text{thn}}^{\text{DL}}}{\left[a_n - \left(\varepsilon a_f + \kappa_{SD_n}^2\right)\gamma_{\text{thn}}^{\text{DL}}\right]\gamma_S}.$$

Proof. See Appendix B. □

The asymptotic OP of D_n in the high-SNR regime is given in the following corollary.

Corollary 2. *The asymptotic OP of D_n in the high-SNR regime is expressed as*

$$\mathrm{P}_{\text{out,nid}}^{D_n,\infty} = 1 - e^{-\frac{W_3^\infty}{\beta_{SD_n}}}, \tag{17}$$

where we have $W_3^\infty = \max\left(W_{3,1}^\infty, W_{3,2}^\infty\right)$. *Furthermore,* $W_{3,1}^\infty$ *and* $W_{3,2}^\infty$ *are respectively given by*

$$W_{3,1}^\infty = \frac{\left(1 + \kappa_{SD_n}^2\right)\left(\sigma_{SD_n}^2 + \varpi_{D_n}\right)\gamma_{\text{thf}}^{\text{DL}}}{a_f - \left(a_n + \kappa_{SD_n}^2\right)\gamma_{\text{thf}}^{\text{DL}}},$$
$$W_{3,2}^\infty = \frac{\left(1 + \kappa_{SD_n}^2\right)\left(\sigma_{SD_n}^2 + \varpi_{D_n}\right)\gamma_{\text{thn}}^{\text{DL}}}{a_n - \left(\varepsilon a_f + \kappa_{SD_n}^2\right)\gamma_{\text{thn}}^{\text{DL}}}.$$

Proof. In the high-SNR regime, the received SINRs of x_f and x_n at D_n are respectively given by

$$\gamma_{D_n}^{x_f,\infty} = \frac{a_f \rho_{SD_n}}{H_{SD_n} - a_f \rho_{SD_n}}, \tag{17}$$
$$\gamma_{D_n}^{x_n,\infty} = \frac{a_n \rho_{SD_n}}{H_{SD_n} + \left(\varepsilon a_f - 1\right)\rho_{SD_n}}. \tag{18}$$

Upon substituting (17) and (18) into (15), and using the PDF and CDF of ρ_i, (17) can be obtained after some mathematical manipulations. □

B. Uplink Transmission

1) OP of U_n: An outage event occurs at U_n, when s_n cannot be decoded at the BS via the $U_n \to S$ link. Thus, the OP of U_n can be expressed as

$$\mathrm{P}_{\text{out,nid}}^{U_n} = \Pr\left(\gamma_{\text{BS}}^{s_n} < \gamma_{\text{thn}}^{\text{UL}}\right), \tag{19}$$

where $\gamma_{\text{thn}}^{\text{UL}}$ denotes the SNR threshold of s_n. The exact OP of U_n is given in the following theorem.

Theorem 3. *The exact OP of U_n is expressed as*

$$\mathrm{P}_{out,nid}^{U_n} = 1 - \frac{\beta_{SU_n}^2}{2\beta_{SS}\left(\beta_{SU_n} + A_1\beta_{SU_f}\right)\left(\beta_{SU_n} + A_2\beta_{LI}\right)} \times \sqrt{\frac{\pi\beta_{SU_n}}{A_3}} e^{\frac{\beta_{SU_n}}{4\beta_{SS}^2 A_3} - \frac{A_4}{\beta_{SU_n}}} \left[1 - \mathrm{erfc}\left(\frac{1}{2\beta_{SS}}\sqrt{\frac{\beta_{SU_n}}{A_3}}\right)\right], \tag{20}$$

where we have $A_1 = \left(1 + \kappa_{SU_f}^2\right)\gamma_{U_f}\phi$, $A_2 = \gamma_S\phi$, $A_3 = \left(1 + \kappa_{SS}^2\right)\delta^2\gamma_S\phi$,

$$A_4 = \phi\left[\left(\sigma_{SU_n}^2 + \varpi_{U_n}\right)\left(1 + \kappa_{SU_n}^2\right)\gamma_{U_n} + 1\right] + A_1\left(\sigma_{SU_f}^2 + \varpi_{U_f}\right) + \sigma_{SS}^2 A_3,$$
$$\phi = \frac{\gamma_{\text{thn}}^{\text{UL}}}{\left(1 - \kappa_{SU_n}^2\gamma_{\text{thn}}^{\text{UL}}\right)\gamma_{U_n}}.$$

Furthermore, we also have $\kappa_{SU_n}^2\gamma_{\text{thn}}^{\text{UL}} < 1$, *otherwise* $\mathrm{P}_{\text{out,nid}}^{U_n} = 1$. *Additionally,* $\mathrm{erfc}\left(\cdot\right)$ *denotes the complementary error function, which is expressed as*

$$\mathrm{erfc}\left(v\right) = \frac{2}{\sqrt{\pi}}\int_v^\infty e^{-t^2}dt. \tag{21}$$

Proof. See Appendix C. □

The asymptotic OP of U_n in the high-SNR regime is given in the following corollary.

Corollary 3. *The asymptotic OP of U_n in the high-SNR regime is expressed as*

$$\mathrm{P}_{\text{out,nid}}^{U_n,\infty} = 1 - \frac{\beta_{SU_n}}{\beta_{SU_n} + A_1^\infty\beta_{SU_f}} e^{-\frac{A_4^\infty}{\beta_{SU_n}}}, \tag{22}$$

where we have

$$A_1^\infty = \frac{\gamma_{\text{thn}}^{\text{UL}}\left(1 + \kappa_{SU_f}^2\right)}{1 - \kappa_{SU_n}^2\gamma_{\text{thn}}^{\text{UL}}},$$
$$A_4^\infty = \left[\left(1 + \kappa_{SU_f}^2\right)\left(\sigma_{SU_f}^2 + \varpi_{U_f}\right) + \left(1 + \kappa_{SU_n}^2\right)\left(\sigma_{SU_n}^2 + \varpi_{U_n}\right)\right] \times \frac{\gamma_{\text{thn}}^{\text{UL}}}{1 - \kappa_{SU_n}^2\gamma_{\text{thn}}^{\text{UL}}}.$$

Proof. In the high-SNR regime, the receive SINR of s_n at U_n is given by

$$\gamma_{\text{BS}}^{s_n,\infty} = \frac{\rho_{SU_n}}{H_{SU_f} + H_{SU_n}}. \tag{23}$$

Upon substituting (23) into (19), and using the PDF as well as CDF of ρ_i, (22) can be obtained after some mathematical manipulations. □

2) OP of U_f: An outage event occurs at U_f, when s_f or s_n cannot be decoded at the BS successfully via the $U_f \to S$ or $U_n \to S$ link. Thus, the OP of U_f can be expressed as

$$\mathrm{P}_{\mathrm{out,nid}}^{U_f} = 1 - \Pr\left(\gamma_{\mathrm{BS}}^{s_n} > \gamma_{\mathrm{thn}}^{\mathrm{UL}}, \gamma_{\mathrm{BS}}^{s_f} > \gamma_{\mathrm{thf}}^{\mathrm{UL}}\right), \tag{24}$$

where $\gamma_{\mathrm{thf}}^{\mathrm{UL}}$ denotes the SNR threshold of s_f. Due to the presence of RHIs and ipSIC, it is challenging to obtain a closed-form expression for the OP of U_f. Thus, we adopt the integral form instead in the following theorem.

Theorem 4. *The exact OP of U_f is expressed as*

$$\begin{aligned}\mathrm{P}_{\mathrm{out,nid}}^{U_f} = 1 - \frac{\beta_{SU_n}^2}{\beta_{SS}} \Bigg\{ & \frac{1}{\left(\beta_{SU_n} + A_1\beta_{SU_f}\right)\left(\beta_{SU_n} + A_2\beta_{LI}\right)} \\ & \times \sqrt{\frac{\pi\beta_{SU_n}}{4A_3}} e^{\frac{\beta_{SU_n}}{4A_3\beta_{SS}^2}} \left[1 - \mathrm{erfc}\left(\frac{1}{\beta_{SS}}\sqrt{\frac{\pi\beta_{SU_n}}{4A_3}}\right)\right] \\ & - \frac{e^{\frac{B_4}{\beta_{SU_n}}}}{\left(\beta_{SU_n} + B_1\beta_{SU_f}\right)\left(\beta_{SU_n} - B_2\beta_{LI}\right)} \int_0^{\infty} e^{\frac{\beta_{SS}B_3t^2 - \beta_{SU_n}t}{\beta_{SU_n}\beta_{SS}}} dt \Bigg\},\end{aligned} \tag{25}$$

where we have $B_2 = \gamma_S\zeta$, $B_3 = \left(1 + \kappa_{SS}^2\right)\delta^2\gamma_S\zeta$,

$$\begin{aligned} B_1 &= \frac{\left(1 - \kappa_{SU_f}^2\gamma_{\mathrm{thf}}^{\mathrm{UL}}\right)\gamma_{U_f}\zeta}{\gamma_{\mathrm{thf}}^{\mathrm{UL}}}, \\ B_4 &= \Big[\left(1 + \kappa_{SU_f}^2\right)\left(\sigma_{SU_f}^2 + \varpi_{U_f}\right)\gamma_{U_f} + \left(1 + \kappa_{SU_n}^2\right) \\ &\quad \times \left(\sigma_{SU_n}^2 + \varpi_{U_n}\right)\gamma_{U_n} + 1\Big]\zeta + \sigma_{SS}^2 B_3, \\ \zeta &= \frac{1}{\left(\kappa_{SU_f}^2 + \varepsilon\right)\gamma_{U_n}}. \end{aligned}$$

Furthermore, we also have $\kappa_{SU_f}^2\gamma_{\mathrm{thf}}^{\mathrm{UL}} < 1$, otherwise $\mathrm{P}_{\mathrm{out,nid}}^{U_f} = 1$.

Proof. See Appendix D. □

The asymptotic OP of U_f in the high-SNR regime is given in the following corollary.

Corollary 4. *The asymptotic OP of U_f in the high-SNR regime is expressed as*

$$\begin{aligned}\mathrm{P}_{\mathrm{out,nid}}^{U_f,\infty} = 1 &- \frac{\beta_{SU_n}}{\beta_{SU_n} + A_1^{\infty}\beta_{SU_f}} e^{-\frac{A_4^{\infty}}{\beta_{SU_n}}} \\ &+ \frac{B_1^{\infty}\beta_{SU_n}}{\beta_{SU_f} + B_1^{\infty}\beta_{SU_n}} e^{\frac{B_4^{\infty}}{B_1^{\infty}\beta_{SU_n}}},\end{aligned} \tag{26}$$

where we have

$$\begin{aligned} B_1^{\infty} &= \frac{\gamma_{\mathrm{thf}}^{\mathrm{UL}}\left(\varepsilon + \kappa_{SU_n}^2\right)}{1 - \kappa_{SU_f}^2\gamma_{\mathrm{thf}}^{\mathrm{UL}}}, \\ B_4^{\infty} &= \Big[\left(1+\kappa_{SU_f}^2\right)\left(\sigma_{SU_f}^2+\varpi_{U_f}\right) + \left(1+\kappa_{SU_n}^2\right)\left(\sigma_{SU_n}^2+\varpi_{U_n}\right)\Big] \\ &\quad \times \frac{\gamma_{\mathrm{thf}}^{\mathrm{UL}}}{1 - \kappa_{SU_f}^2\gamma_{\mathrm{thf}}^{\mathrm{UL}}}. \end{aligned}$$

Remark 2. *It can be observed from (11) and (16) that both the RHIs and the CEEs as well as ipSIC reduce the SINRs of the desired signal decoded at the communication RXs. This potentially erodes the communication performance of the system considered. Moreover, it should be pointed out that if the RHIs, CEEs, and ipSIC reduce to 0, the system considered operates in ideal conditions. Upon substituting $\kappa = \sigma = \varepsilon = 0$ into the Theorems and Corollaries, the exact and asymptotic OPs of the IoT devices can be obtained, respectively. Specifically, the closed-form expression of the OP of U_f in ideal conditions is formulated in (27), which is shown at the top of the next page, where $\phi' = \gamma_{\mathrm{thn}}^{\mathrm{UL}}/\gamma_{U_n}$, $\varsigma' = \gamma_{\mathrm{thf}}^{\mathrm{UL}}/\gamma_{U_f}$, $\psi = \delta^2\phi'\gamma_S\left(\beta_{SU_f} + \varsigma'\gamma_{U_f}\right)$, and $\varpi = \varpi_{U_f}\gamma_{U_f} + \varpi_{U_n}\gamma_{U_n} + 1$. Furthermore, in the context of fixed total power consumption, if the number of UL or DL IoT devices is increased, the capability of the communication RXs to decode the expected signals is degraded, which further reduces the outage performance.*

IV. Sensing Performance

In this section, the PoD $\mathrm{P_d}$ of the BS is derived for evaluating the sensing performance of the FD NO-T ISAC system considered. The PoD represents the probability that the RXs successfully detect the presence of targets. By contrast, the probability of false alarm (PoFA) $\mathrm{P_{fa}}$ refers to the RXs making the decision that a target is within the sensing range, when this is not the case. Specifically, PoFA and PoD can be mathematically reduced to a binary detection problem, i.e., $\mathrm{P_{fa}} = \Pr\left(\mathcal{H}_1 | \mathcal{H}_0\right)$ and $\mathrm{P_d} = \Pr\left(\mathcal{H}_1 | \mathcal{H}_1\right)$, where $\mathcal{H}_1$ and $\mathcal{H}_0$ respectively represent the alternative target present/absent hypothesis. This may be rephrased as to whether the signals received by the RXs do or do not contain target echos. Uniquely for such scenarios, the alternative and null hypotheses of the FD NO-T ISAC system considered can be respectively defined as [45]

$$\begin{aligned} \mathcal{H}_0: & y_{\mathrm{BS}} = \left(h_{SU_f} + w_{U_f}\right)\left(y_{U_f} + \eta_{SU_f}\right) + \left(h_{SU_n} + w_{U_n}\right) \\ & \times \left(y_{U_n} + \eta_{SU_n}\right) + \left(\delta e_{SS} + h_{LI}\right) y_S + \delta h_{SS}\eta_{SS} + n_S, \\ \mathcal{H}_1: & y_{\mathrm{BS}} = \left(h_{SU_f} + w_{U_f}\right)\left(y_{U_f} + \eta_{SU_f}\right) + \left(h_{SU_n} + w_{U_n}\right) \\ & \times \left(y_{U_n} + \eta_{SU_n}\right) + \delta h_{SS}\left(y_S + \eta_{SS}\right) + h_{LI}y_S + n_S. \end{aligned} \tag{28}$$

According to the Neyman-Pearson criterion [46], the PoD can be maximized at a fixed PoFA. Furthermore, it can be seen from (28) that the power received at the BS obeys distribution the non-central Chi-square having five degrees-of-freedom (DoFs) under $\mathcal{H}_0$ and $\mathcal{H}_1$. Thus, $\mathrm{P_{fa}}$ and $\mathrm{P_d}$ of the system considered can be respectively expressed as (30) and (31), shown at the top of the next page [47], where ξ is the detection threshold and $Q\left(\cdot,\cdot\right)$ denotes the Marcum Q-function. Moreover, $P_{\mathrm{i+n}}$ is further expressed as

$$\begin{aligned} P_{\mathrm{i+n}} = & \kappa_{SU_f}^2 P_{U_f}\left(\varpi_{U_f} + \left|h_{SU_f}\right|^2\right) + \left|\delta h_{SS}\right|^2\kappa_{SS}^2 P_S \\ & + \kappa_{SU_n}^2 P_{U_n}\left(\varpi_{U_n} + \left|h_{SU_n}\right|^2\right) + N_0. \end{aligned} \tag{29}$$

Remark 3. *In combination with (11), (16), (20), (26), and (31), we can observe that the C&S performances are mutually restricted in the FD NO-T ISAC system considered. It can also be observed that the RHIs and CEEs mislead the sensing*

$$\mathrm{P}_{\mathrm{out,id}}^{U_f} = 1 - \frac{\beta_{SU_n}^2 \beta_{SU_f}}{2\beta_{SS}\left(\beta_{SU_f}\gamma_{U_f}\phi' + \beta_{SU_n}\right)\left[\beta_{SU_f}\beta_{LI}\gamma_S\phi'\left(\varsigma'\gamma_{U_f}+1\right) + \beta_{SU_n}\beta_{LI}\gamma_S\varsigma' + \beta_{SU_f}\beta_{SU_n}\right]} \times \sqrt{\frac{\pi}{\psi}}\left[1 - \mathrm{erfc}\left(\frac{1}{2\beta_{SS}}\sqrt{\frac{1}{\psi}}\right)\right] e^{\frac{1}{4\psi\beta_{SS}^2}} - \frac{\varpi\left(\phi'\varsigma'\beta_{SU_f}\gamma_{U_f} + \varsigma'\beta_{SU_n} + \phi'\beta_{SU_f}\right)}{\beta_{SU_f}\beta_{SU_n}}}. \tag{27}$$

$$\mathrm{P}_{\mathrm{fa}} = Q_{\frac{5}{2}}\left(\sqrt{\frac{2\left(H_{SU_f}P_{U_f} + H_{SU_n}P_{U_n} + \left(\delta^2\sigma_{SS}^2 + \rho_{LI}\right)P_S\right)}{P_{\mathrm{i+n}}}}, \sqrt{\frac{2\xi}{P_{\mathrm{i+n}}}}\right), \tag{30}$$

$$\mathrm{P}_{\mathrm{d}} = Q_{\frac{5}{2}}\left(\sqrt{\frac{2\left(H_{SU_f}P_{U_f} + H_{SU_n}P_{U_n} + \left(\delta^2 H_{SS} + \rho_{LI}\right)P_S\right)}{P_{\mathrm{i+n}}}}, \sqrt{\frac{2\xi}{P_{\mathrm{i+n}}}}\right), \tag{31}$$

RX into making false decisions, which reduces the PoD of the ISAC system considered. In addition, the increase of the number of UL IoT devices aggravates the negative impact of multi-path on the sensing RX, which reduces the PoD of the BS. Furthermore, it can be observed that the increase of the UL transmit power imposes undesired effects both on the sensing and on the DL IoT RXs. By contrast, increasing the transmit power of the BS causes severe LSI, which degrades the outage performance of UL IoT devices. Hence, finding the most appropriate PA scheme for the BS and UL IoT TXs is of pivotal significance, which inspires the subsequent investigations of this paper.

V. Power Allocation Scheme

In this section, a communication-centric PA problem is formulated, so that the resource utilization of the FD NO-T ISAC system can be improved. Specifically, the proposed PA scheme maximizes the sum-rate of the UL and DL IoT devices, while guaranteeing a certain sensing capability for the system. In general, three types of optimization problems are considered for ISAC system, i.e., CCD [22], sensing-centric design (SCD) [34], and joint communication and sensing design (JCSD) [17]. These three designs tend to result in different emphases and apply to different scenarios. As a challenging ambition, we design a FD UL-DL NO-T ISAC system, with an emphasis on the CCD design philosophy in this paper. Both SCD and JCSD are meaningful, which will be set aside for our future work.

A. Problem Formulation

The sum rate of our FD NO-T ISAC system is expressed as [37]

$$R_{\mathrm{sum}} = R_{s_f} + R_{s_n} + R_{x_f} + R_{x_n}, \tag{32}$$

where R_{s_f}, R_{s_n}, R_{x_f}, and R_{x_n} denote the data rates of s_f, s_n, x_f, and x_n, and are respectively given by [48]

$$R_{s_f} = \log_2\left(1 + \gamma_{\mathrm{BS}}^{s_f}\right), \tag{33}$$

$$R_{s_n} = \log_2\left(1 + \gamma_{\mathrm{BS}}^{s_n}\right), \tag{34}$$

$$R_{x_f} = \log_2\left[1 + \min\left(\gamma_{D_n}^{x_f}, \gamma_{D_f}^{x_f}\right)\right], \tag{35}$$

$$R_{x_n} = \log_2\left(1 + \gamma_{D_n}^{x_n}\right). \tag{36}$$

In light of the above, the communication-centric PA scheme can be formulated as

$$\max_{P_{U_n}, P_{U_f}, P_S, a_f, a_n} R_{\mathrm{sum}} \tag{37}$$

$$\text{s.t. } \delta^2\rho_{SS}P_S - \alpha P_{\mathrm{RCLN}} \geqslant P_{\mathrm{th}}, \tag{37a}$$

$$\gamma_{\mathrm{BS}}^{s_n} \geqslant \gamma_{\mathrm{thn}}^{\mathrm{UL}}, \gamma_{\mathrm{BS}}^{s_f} \geqslant \gamma_{\mathrm{thf}}^{\mathrm{UL}}, \min\left(\gamma_{D_f}^{x_f}, \gamma_{D_n}^{x_f}\right) \geqslant \gamma_{\mathrm{thf}}^{\mathrm{DL}}, \gamma_{D_n}^{x_n} \geqslant \gamma_{\mathrm{thn}}^{\mathrm{DL}}, \tag{37b}$$

$$0 \leqslant P_{U_f} < P_{U_n} \leqslant P_{\max}^{\mathrm{UL}}, 0 \leqslant P_S \leqslant P_{\max}^{\mathrm{DL}}, \tag{37c}$$

$$a_n + a_f = 1,\ 0 < a_n < a_f < 1, \tag{37d}$$

where (37a) represents that the received power of the target echo, of the interference, and of the noise at the BS satisfy a specific condition in support of sensing. The constraint (37b) indicates that s_f, s_n, x_f, and x_n can be successfully decoded for communication, while (37c) represents the power budget of the UL and DL TXs. Finally, (37d) represents the constraints of the NO-DLT protocol [13], [40]. Furthermore, $\alpha \geqslant 0$ in (37a) is the regularization parameter and P_{RCLN} represents the power of the RHIs, CEEs, LSI, noise as well as the signals transmitted from the UL IoT TXs, which is given by

$$P_{\mathrm{RCLN}} = H_{SU_f}P_{U_f} + \left(H_{SU_n} + \rho_{SU_n}\right)P_{U_n} + P_S\left[\delta^2\left(\sigma_{SS}^2 + \kappa_{SS}^2|h_{SS}|^2\right) + \rho_{LI}\right] + N_0. \tag{38}$$

Remark 4. *It should be emphasized that (37a) is essentially equivalent to the constraint on the SINR of the echo signal. Actually, after some basic mathematical manipulations, (37a) can be further rewritten as*

$$\delta^2\rho_{SS}P_S - \alpha P_{\mathrm{RCLN}} \geq P_{\mathrm{th}} \Leftrightarrow \frac{\delta^2\rho_{SS}P_S}{P_{\mathrm{RCLN}}} \geq \gamma_{\mathrm{th}}^{\mathrm{d}}, \tag{39}$$

where we have $\gamma_{\mathrm{th}}^{\mathrm{d}} = P_{\mathrm{th}}/P_{\mathrm{RCLN}} + \alpha$. Furthermore, it can be observed that the PoD can be improved by increasing the SINR of the echo according to (31). To this end, (37a) can be ascribed to the constraint of PoD.

Upon substituting (4)-(6), (8), (9), and (33)-(36) into (37), and introducing the slack variable Δ, our optimization problem

in (37) can be rewritten as

$$\mathcal{P}1: \max_{P_{U_n},P_{U_f},P_S,a_f,a_n} \ \frac{1}{\ln 2}\left(\Omega+\Delta\right) \tag{40}$$

$$\text{s.t. } \Delta \leqslant \ln\Delta_1 - \ln\Delta_2,\ \Delta \leqslant \ln\Delta_3 - \ln\Delta_4, (37a)-(37d), \tag{40a}$$

where $\Omega = \ln\Omega_1 - \ln\Omega_2 + \ln\Omega_3 - \ln\Omega_4 + \ln\Omega_5 - \ln\Omega_6$, $\Omega_2 = \Omega_1 - \rho_{SU_f}P_{U_f}$, $\Omega_4 = \Omega_3 - \rho_{SU_n}P_{U_n}$, $\Omega_6 = \Omega_5 - a_n\rho_{SD_n}P_S$, $\Delta_2 = \Delta_1 - a_f\rho_{SD_f}P_S$, and $\Delta_4 = \Delta_3 - a_f\rho_{SD_n}P_S$. While Ω_1, Ω_3, Ω_5, Δ_1, and Δ_3 are respectively expressed as

$$\Omega_1 = H_{SU_f}P_{U_f} + (H_{SU_n} + \varepsilon\rho_{SU_n})P_{U_n} + (H_{SS}\delta + \rho_{LI})P_S + N_0, \tag{41}$$

$$\Omega_3 = H_{SU_f}P_{U_f} + (H_{SU_n} + \rho_{SU_n})P_{U_n} + (H_{SS}\delta + \rho_{LI})P_S + N_0, \tag{42}$$

$$\Omega_5 = [H_{SD_n} + (\varepsilon-1)a_f\rho_{SD_n}]P_S + H_{fn}P_{U_f} + H_{nn}P_{U_n} + N_0, \tag{43}$$

$$\Delta_1 = H_{SD_f}P_S + H_{ff}P_{U_f} + H_{nf}P_{U_n} + N_0, \tag{44}$$

$$\Delta_3 = H_{SD_n}P_S + H_{fn}P_{U_f} + H_{nn}P_{U_n} + N_0. \tag{45}$$

It can be observed from (40) that the PA coefficients are interdependent, and it is difficult to optimize them simultaneously. Fortunately, we find that this dilemma can be resolved by fixing either (P_{U_f}, P_{U_n}, P_S) or (a_n, a_f). Therefore, an alternating optimization algorithm is proposed for addressing $\mathcal{P}1$ near-optimally. Specifically, $\mathcal{P}1$ is divided into two sub-problems, i.e.,

$\mathcal{P}1.1$: Optimize P_{U_f}, P_{U_n}, and P_S at a fixed a_n and a_f;

$\mathcal{P}1.2$: Optimize a_n and a_f at a fixed P_{U_f}, P_{U_n}, and P_S.

B. Optimization of P_S, P_{U_f}, and P_{U_n}

For the given a_n and a_f, $\mathcal{P}1$ can be reduced to[4]

$$\mathcal{P}1.1: \max_{P_{U_n},P_{U_f},P_S} \ \Omega+\Delta \tag{46}$$

$$\text{s.t. } \Delta \leqslant \ln\Delta_1 - \ln\Delta_2,\ \Delta \leqslant \ln\Delta_3 - \ln\Delta_4, (37a)-(37c), \tag{46a}$$

We can observe that $\mathcal{P}1.1$ is still challenging to solve due to the non-convexity of the negative logarithmic functions, namelys $-\ln\Omega_2$, $-\ln\Omega_4$, $-\ln\Omega_6$, $-\ln\Delta_2$, and $-\ln\Delta_4$ in (46) and (46a). To this end, we adopt the following function to tackle this challenge

$$g(t) = -tx + \ln t + 1,\ t > 0. \tag{47}$$

It can be inferred from (47) that if and only if $t^* = 1/x$, the maximum of $g(t)$ can be obtained, i.e., $-\ln x = \max_{t>0} g(t)$. In this way, (46) can be reformulated as (48), shown at the top of the next page, where we have $g(t_1) = -t_1\Omega_2 + \ln t_1 + 1$, $g(t_2) = -t_2\Omega_4 + \ln t_2 + 1$, $g(t_3) = -t_3\Omega_6 + \ln t_3 + 1$, $g(t_4) = -t_4\Delta_2 + \ln t_4 + 1$, $g(t_5) = -t_5\Delta_4 + \ln t_5 + 1$.

[4]To simplify the analysis, $1/\ln 2$ in (40) is ignored, but this has no effect on the PA coefficients.

Observe that the optimization sub-problem (48) is convex, and the optimal t_1, t_2, t_3, t_4, and t_5 are respectively given by

$$t_1^* = \left(H_{SU_f}P_{U_f} + H_{SU_n}P_{U_n} + H_{SS}\delta P_S + \rho_{LI}P_S + N_0\right)^{-1}, \tag{49}$$

$$t_2^* = \left[\left(H_{SU_f} - \rho_{SU_f}\right)P_{U_f} + \left(H_{SU_n} + \varepsilon\rho_{SU_n}\right)P_{U_n} + \left(H_{SS}\delta + \rho_{LI}\right)P_S + N_0\right]^{-1}, \tag{50}$$

$$t_3^* = \left[\left(H_{SD_n} + (\varepsilon a_f - 1)\rho_{SD_n}\right)P_S + H_{fn}P_{U_f} + H_{nn}P_{U_n} + N_0\right]^{-1}, \tag{51}$$

$$t_4^* = \left[\left(H_{SD_f} - a_f\rho_{SD_f}\right)P_S + H_{ff}P_{U_f} + H_{nf}P_{U_n} + N_0\right]^{-1}, \tag{52}$$

$$t_5^* = \left[\left(H_{SD_n} - a_f\rho_{SD_n}\right)P_S + H_{fn}P_{U_f} + H_{nn}P_{U_n} + N_0\right]^{-1}. \tag{53}$$

Upon substituting t_1^*, t_2^*, t_3^*, t_4^*, and t_5^* into (48), $\mathcal{P}1.1$ can be efficiently solved by using the popular CVX toolbox.

C. Optimization of a_n and a_f

For the given P_S, P_{U_f}, and P_{U_n}, $\mathcal{P}1$ can be reduced to

$$\mathcal{P}1.2: \max_{a_n,a_f} \ \Omega+\Delta \tag{54}$$

$$\text{s.t. } a_n + a_f = 1,\ 0 < a_n < a_f < 1. \tag{54a}$$

Then, similar to $\mathcal{P}1.1$, with the aid of (47), we can rewrite (54) as[5]

$$\mathcal{P}1.2: \max_{a_n,a_f} \ \left\{\ln\Omega_5 + \max g(t_6^*) + \Delta\right\} \tag{55}$$

$$\text{s.t. } \Delta \leqslant \left\{\ln\Delta_1 + \max g(t_7^*)\right\}, \Delta \leqslant \left\{\ln\Delta_2 + \max g(t_8^*)\right\}, (54a), \tag{55a}$$

where we have $g(t_6^*) = -t_6^*\Omega_6 + \ln t_6^* + 1$, $g(t_7^*) = -t_7^*\Delta_2 + \ln t_7^* + 1$, and $g(t_8^*) = -t_8^*\Delta_4 + \ln t_8^* + 1$. Furthermore, t_6^*, t_7^*, and t_8^* are respectively expressed as

$$t_6^* = \left[(H_{SD_n} + (\varepsilon a_f - 1)\rho_{SD_n})P_S + H_{fn}P_{U_f} + H_{nn}P_{U_n} + N_0\right]^{-1}, \tag{56}$$

$$t_7^* = \left[\left(H_{SD_f} - a_f\rho_{SD_f}\right)P_S + H_{ff}P_{U_f} + H_{nf}P_{U_n} + N_0\right]^{-1}, \tag{57}$$

$$t_8^* = \left[\left(H_{SD_n} - a_f\rho_{SD_n}\right)P_S + H_{fn}P_{U_f} + H_{nn}P_{U_n} + N_0\right]^{-1}. \tag{58}$$

It can be confirmed that the optimization sub-problem (55) is convex, and $\mathcal{P}1.2$ can be efficiently solved by using the CVX toolbox.

The alternate optimization procedure is summarized in Algorithm 1, which iteratively finds the near-optimal PA coefficients.

Remark 5. *In the FD NO-T ISAC system considered, higher power is required to minimize the negative effects of the RHIs, CEEs, and ipSIC on the premise of guaranteeing C&S performances. Furthermore, the computational complexity orders of $\mathcal{P}1.1$ and $\mathcal{P}1.2$ respectively are $\mathcal{O}(81L_1)$ and $\mathcal{O}(L_2)$, where L_1 and L_2 denote the number of iterations for $\mathcal{P}1.1$ and $\mathcal{P}1.2$, respectively [49]. We conclude that the overall computational*

[5]It should be pointed out that for a fixed P_S, P_{U_f}, and P_{U_n}, Ω_1, Ω_2, Ω_3, and Ω_4 are all constants. Thus, we leave them out for simplify.

$$\mathcal{P}1.1: \max_{P_{U_n},P_{U_f},P_S,t_1,t_2,t_3} \{\ln\Omega_1 + \max g(t_1) + \ln\Omega_3 + \max g(t_2) + \ln\Omega_5 + \max g(t_3)\} \tag{48}$$

$$\text{s.t. } \Delta \leqslant \{\ln\Delta_1 + \max g(t_4)\},\ \Delta \leqslant \{\ln\Delta_3 + \max g(t_5)\}, \tag{48a}$$

$$t_1 > 0, t_2 > 0, t_3 > 0, t_4 > 0, t_5 > 0, (37a) - (37c), \tag{48b}$$

Algorithm 1: Alternate Optimization Algorithm

input : the maximum number of iterations L and $\lambda > 0$

output: the optimal PA coefficients $P_{U_f}(\ell)$, $P_{U_n}(\ell)$, $P_S(\ell)$, $a_n(\ell)$, and $a_f(\ell)$

Initialize $P_{U_f}(1)$, $P_{U_n}(1)$, $P_S(1)$, $a_n(1)$, and $a_f(1)$ according to (37c) and (37d)
Set $\ell = 1$
repeat
  Set $m = 1$
  repeat
    For the fixed $P_{U_f}(m)$, $P_{U_n}(m)$, and $P_S(m)$, identify the optimal $t_1^*(m)$, $t_2^*(m)$, $t_3^*(m)$, $t_4^*(m)$, and $t_5^*(m)$ according to (49)-(53), respectively
    Solve (48) for given $t_1^*(m)$, $t_2^*(m)$, $t_3^*(m)$, $t_4^*(m)$, and $t_5^*(m)$ and denote the solution as $P_{U_f}(m+1)$, $P_{U_n}(m+1)$, and $P_S(m+1)$
    Update $m = m + 1$
  until *the objective value of (48) reaches convergence*;
  Set $p = 1$
  repeat
    For the given $a_n(p)$ and $a_f(p)$, identify the optimal $t_6^*(p)$, $t_7^*(p)$, and $t_8^*(p)$ according to (56)-(58), respectively
    Solve (55) for given $t_6^*(p)$, $t_7^*(p)$, and $t_8^*(p)$ and denote the solution as $a_n(p+1)$ and $a_f(p+1)$
    Update $p = p + 1$
  until *the objective value of (55) reaches convergence*;
  Update $\ell = \ell + 1$
until $R_{\text{sum}}(\ell) - R_{\text{sum}}(\ell-1) \leqslant \lambda$ *or* $\ell = L$;

complexity of Algorithm 1 is $\mathcal{O}(L_3(81L_1 + L_2))$*, where* L_3 *is the number of iteration required for achieving final convergence.*

VI. Numerical Results

In this section, numerical results are provided by Monte-Carlo computer simulations to demonstrate the accuracy of the theoretical analysis and the effectiveness of the optimization algorithms detailed in Sections III-V. Unless otherwise specified, we consider two UL and two DL IoT devices in the FD NO-T ISAC system considered, where we set $\kappa_{SD_f} = \kappa_{SD_n} = \kappa_{SU_f} = \kappa_{SU_n} = \kappa_{SS} = \kappa_{ff} = \kappa_{nf} = \kappa_{fn} = \kappa_{nn} = \kappa$ and $\sigma_{SD_f} = \sigma_{SD_n} = \sigma_{SU_f} = \sigma_{SU_n} = \sigma_{ff} = \sigma_{nf} = \sigma_{fn} = \sigma_{nn} = \sigma$. The detailed simulation parameters are displayed in Table II [41], [50].

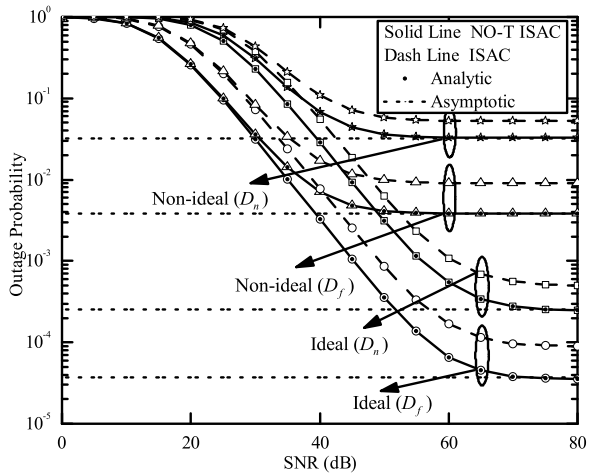

Fig. 2: OPs of the DL IoT RXs vs. the receive SNR.

Fig. 2 plots the OPs of the DL IoT RXs versus the receive SNR for P_{U_n} = 20 dBm and $P_{U_f} = 0.2P_{U_n}$ in the non-ideal ($\kappa = \varepsilon = \sigma = 0.1$) condition. Furthermore, the OPs in the ideal condition ($\kappa = \varepsilon = \sigma = 0$), which corresponds to Remark 2, is presented as well for comparison. The perfect match between the Monte-Carlo simulation results and theoretical analysis demonstrates the accuracy of the derivations in (11) and (16). Moreover, the close approximation of the asymptotic and Monte-Carlo simulation curves in the high-SNR regime is revealed by the derivations in (12) and (17). It can be observed from Fig. 2 that the OPs of the DL IoT RXs decreases upon increasing of the transmit power of the BS in the low and medium-SNR regimes. Nevertheless, due to the detrimental influence of RHIs, CEEs, ipSIC, and the UL-to-DL CCI, OP error floors emerge in the high-SNR regime. Furthermore, compared to the pure ISAC system, the proposed NO-T ISAC exhibits excellent OP performance gains for the DL IoT RXs.

Fig. 3 illustrates the OPs of the UL IoT TXs versus the receive SNR for P_S = 20 dBm and $P_{U_f} = 0.2P_{U_n}$ both in the ideal and non-ideal conditions. The coincidence and close approximation of the Monte-Carlo curves with our theoretical analysis and with the asymptotic curves, respectively, prove the accuracy of our derivations in (20), (22), and (26). In contrast to the NO-DLT, the OP of the near UL TX is inferior to that

TABLE II: Simulation parameters

Parameter	Value	Parameter	Value	Parameter	Value	Parameter	Value
d_{SU_f}, d_{SD_f}	100 m	d_{SU_n}, d_{SD_n}, d_{nn}	10 m	d_{ST}, d_{TS}	50 m	d_{fn}, d_{nf}	95 m
κ	0.1	ε	0.1	σ	0.1	υ	2
$\gamma_{\text{thf}}^{\text{UL}}$, $\gamma_{\text{thf}}^{\text{DL}}$	1.3 dB	$\gamma_{\text{thn}}^{\text{UL}}$, $\gamma_{\text{thn}}^{\text{DL}}$	3.1 dB	β_{LI}	0.1	δ	0.9
ϖ_{D_f}, ϖ_{D_n}	0.01	ϖ_{U_f}, ϖ_{U_n}	0.01	N_0	1	α	1
a_f	0.8	a_n	0.2	P_{th}	1	P_{fa}	10^{-6}
λ	10^{-3}	L	40				

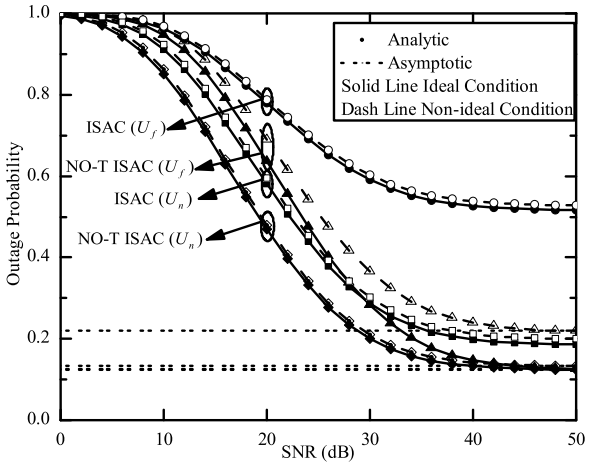

Fig. 3: OPs of the UL IoT TXs vs. the receive SNR.

of the far TX, which is due to the low transmit power and poor channel condition of the far UL IoT TX. As expected, RHIs, CEEs, and ipSIC increase the OP of the UL IoT TXs.

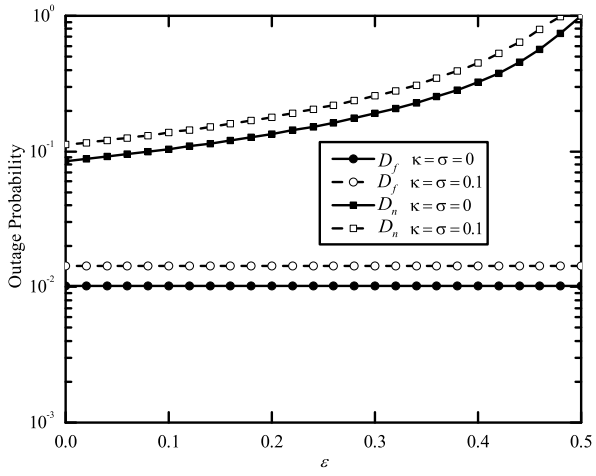

Fig. 4: OPs of the DL IoT RXs vs. ipSIC.

Fig. 4 presents the OPs of the DL IoT RXs versus the ipSIC coefficient ε for P_S = 35 dBm, P_{U_n} = 20 dBm, and $P_{U_f} = 0.2P_{U_n}$. Observe from Fig. 4 that the OP of the far DL IoT RX is independent of the ipSIC coefficient, since only the desired signal is decoded without the SIC being executed at D_f. For the near DL IoT device, the OP increases as the SIC performance degrades. Moreover, it is worth noting that ε can be increased to 1 theoretically, due to that, however, as mentioned in Section III, then $a_n > \left(\varepsilon a_f + \kappa_{SD_n}^2\right)\gamma_{\text{thn}}^{\text{DL}}$ must be satisfied consistently and the OP of D_n already becomes 100% when $\varepsilon = 0.5$.

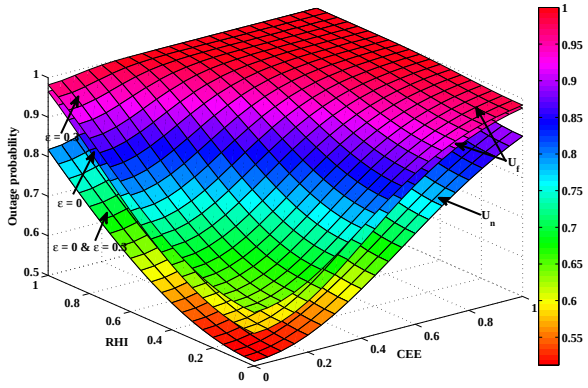

Fig. 5: OPs of the UL IoT TXs vs. RHIs and CEEs.

Fig. 5 depicts the OPs of the UL IoT TXs versus the RHIs κ and CEEs σ for $P_S = P_{U_n}$ = 20 dBm and $P_{U_f} = 0.5P_{U_n}$. It can be seen that CEEs, RHIs, and ipSIC all degrade the outage performance of the IoT devices. As a benefit of the high transmit power and superb channel condition, the OP of the near UL IoT TX is better than that of the far UL IoT TX. As for the UL transmission, since the signal detection of the near IoT TX dispenses with SIC at the BS, the 3D plots of the OP for $\varepsilon = 0$ and $\varepsilon = 0.3$ are identical. From the area of color distribution reel in Fig. 5, it may be concluded that the OPs of the IoT TXs in the system considered are more sensitive to CEEs than to RHIs.

Fig. 6 displays the PoD of the system versus the BS transmit power for P_{U_n} = 15 dBm and $P_{U_f} = 0.2P_{U_n}$. Notably, the sensing behavior can be improved upon increasing the transmit power of the BS. It can be inferred from Fig. 6 that both the RHIs and CEEs degrade the sensing capability of the BS. As for the communication function, the RHIs engender a more grave PoD degradation compared to CEEs. Furthermore, we can also observe that in the context of the same PoD, the pure ISAC system consumes higher transmit power than the NO-T ISAC system proposed. The results further confirm the superiority of the proposed NO-T ISAC scheme in terms of

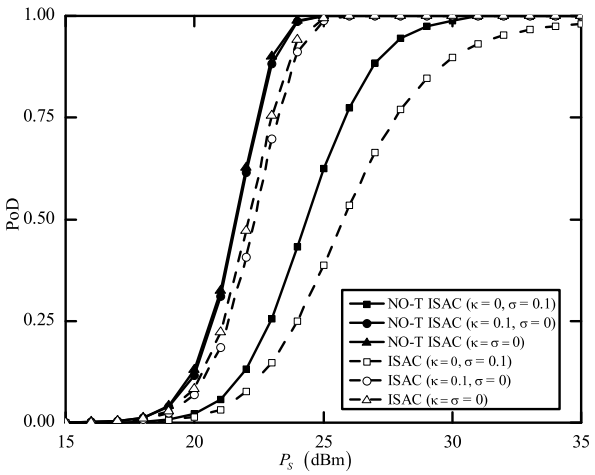

Fig. 6: PoD vs. the transmit power of S.

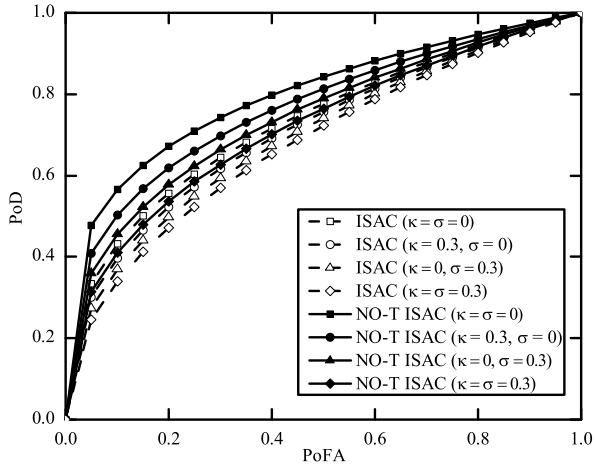

Fig. 7: PoD vs. PoFA.

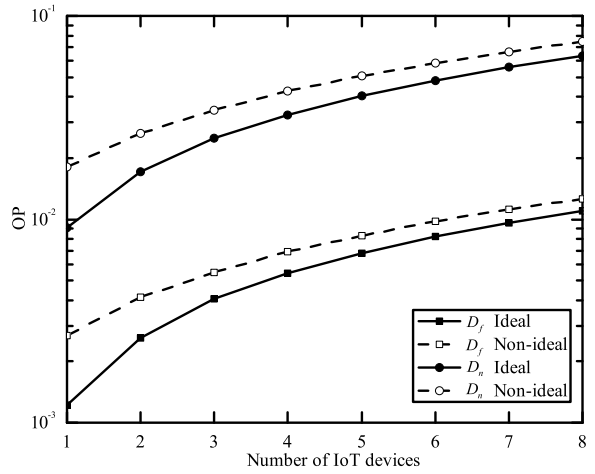

Fig. 8(a): OPs of the DL IoT RXs vs. the number of IoT devices.

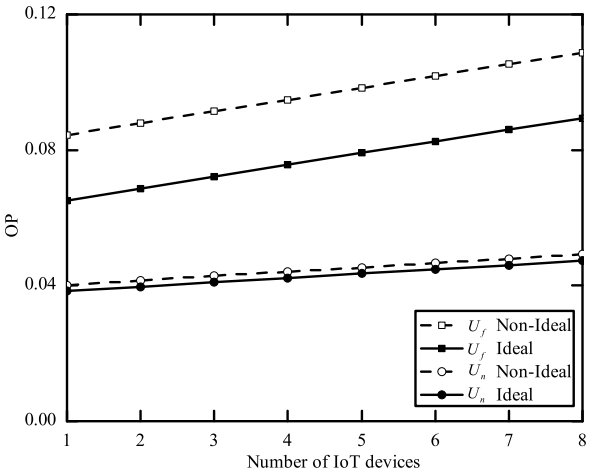

Fig. 8(b): OPs of the UL IoT RXs vs. the number of IoT devices.

the PoD in sensing.

Fig. 7 investigates the PoD of the system versus the PoFA for P_{U_f} = 10 dBm, P_{U_n} = 15 dBm, and P_S = 30 dBm. The sensing performance of the BS is characterized by the ROC curves and the area under the curve (AUC) confirm our inference from Fig. 6. As an innovative contribution, we conclude that the introduction of NO-T into our ISAC system alleviates the detrimental effects of RHIs and CEEs to a certain extent.

Fig. 8 expands the OPs of D_n, D_f, U_n, and U_f and the PoD of the system versus the number of IoT devices both in ideal and non-ideal conditions. Specifically, Fig. 8(a) and 8(b) show the OPs of the DL and UL users which are farthest and closest to the BS, respectively, and Fig. 8(c) shows the PoD of the BS in the multi-IoT device scenario. From Fig. 8(a), we can observe that the OP of the DL IoT devices are increased upon increasing the number of IoT devices, which is because the transmit power allocated by the IoT device decreases, and the interference impinging from the UL IoT devices increases. It can be observed from Fig. 8(b) and 8(c) that the OP of the UL IoT devices and the PoD of the BS are degraded with the increase of the number of IoT device. These trends indicate that increasing the number of the IoT devices increases the negative impact of multi-path propagation, thereby further reducing the C&S performance.

Fig. 9 demonstrates the convergence of the proposed algorithm in terms of its sum rate both in ideal and non-ideal conditions. Observe from Fig. 9 that the proposed algorithm converges to the near-optimal solution of (37). It can be seen from Fig. 9 that the RHIs, CEEs, and ipSIC imperfections

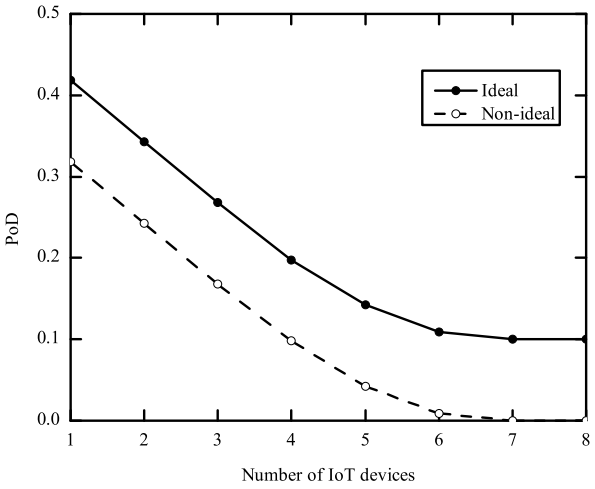

Fig. 8(c): PoD vs. the number of IoT devices.

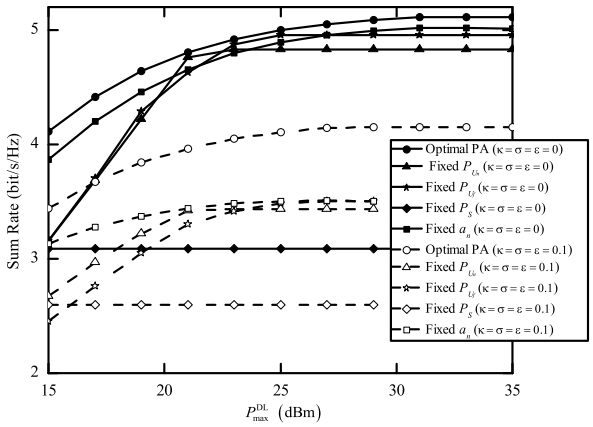

Fig. 10: Sum rate vs. the maximum transmit power of the BS.

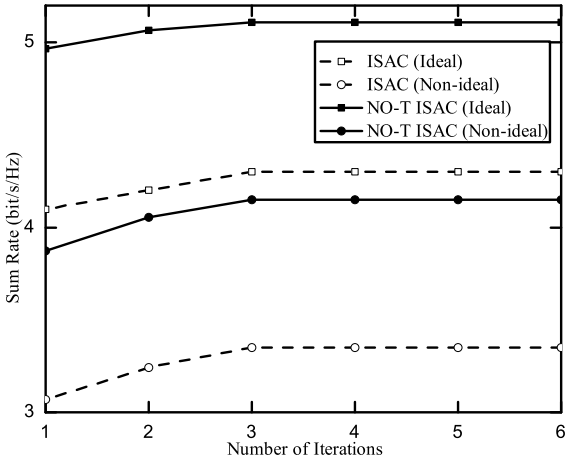

Fig. 9: Convergence of the proposed near-optimal PA algorithm.

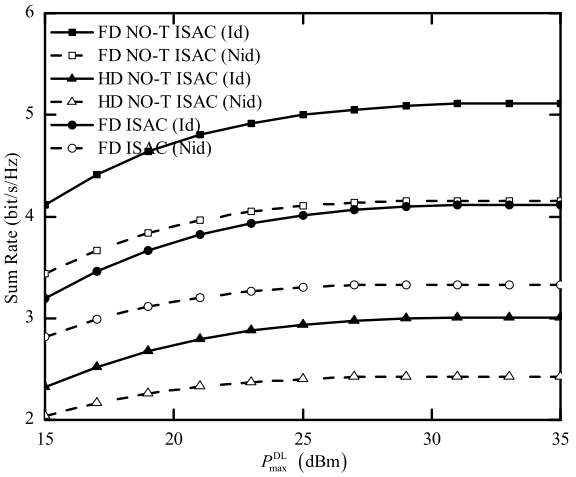

Fig. 11: Sum rate vs. the maximum transmit power of the BS in the different modes.

lead to sum rate reduction for both UL TXs and DL RXs. As a further step, we also confirm that the NO-T ISAC system considered outperforms the pure ISAC system as regards to its sum rate.

Fig. 10 shows the sum rate of the UL TXs and DL RXs vs. the maximum transmit power of the BS in both ideal and non-ideal conditions. In order to highlight the superiority of the proposed algorithm, we provide four other baseline schemes for comparison having fixed P_{U_f}, fixed P_{U_n}, fixed P_S, and fixed a_n. Evidently, the proposed near-optimal PA scheme exhibits outstanding performance in terms of its sum rate compared to the other baseline schemes. The reasons for this phenomenon can be explained as follows: 1) For the fixed P_{U_f} or P_{U_n}, the LSI and CCI cannot be sufficiently suppressed. 2) For the fixed P_S, the relationship is not well balanced between LSI and the signals received from the UL IoT devices as well as the target echo. 3) For the fixed a_n, the PA coefficients transmitted to the DL IoT devices are constant, and the SIC cannot be optimally configured at the RXs.

Fig. 11 plots the sum rate of the UL TXs and DL RXs in both ideal ($\kappa = \sigma = \varepsilon = 0$) and non-ideal ($\kappa = \sigma = \varepsilon = 0.1$) conditions by employing the near-optimal PA scheme. For comparison, the sum rate of the HD mode is presented as well. We can observe conceived from Fig. 10 that the proposed FD NO-T ISAC scheme outperforms both HD NO-T ISAC and FD pure ISAC schemes. It is worth noting that the sum rate of the FD mode is almost twice that of HD, which is due to the fact that signals are transmitted and received simultaneously in the FD mode, whereas the HD mode requires two separate time slots. Furthermore, we can also observe that LSI limits the sum rate in the FD mode.

VII. Conclusions

A FD NO-T ISAC system was conceived, in which the BS simultaneously can perform communication and target sensing. To be practical, the RHIs, CEEs, and ipSIC were taken into account. Both the exact and asymptotic OPs of the UL IoT TXs and DL IoT RXs as well as the PoD of the BS, were derived respectively, in order to evaluate the performance of C&S. Additionally, a communication-centric PA scheme was designed for further enhancing the resource utilization. We first transformed the non-convex problem formulated into a convex one, and then conceived an iterative algorithm for optimally solving the problem. The simulation results confirmed that the NO-T ISAC system considered yields compelling benefits over the pure ISAC system. Moreover, the C&S performance was limited by both the RHIs and CEEs. Finally, we demonstrated the effectiveness of the proposed PA scheme in improving the system's sum rate, while satisfying the sensing requirements.

Appendix A: Proof of Theorem 1

Upon substituting (5) into (10), the OP of D_f can be rewritten as

$$\begin{aligned}\mathrm{P}_{\text{out,nid}}^{D_f} &= \Pr\left(\frac{a_f\rho_{SD_f}\gamma_S}{\left(H_{SD_f}-a_f\rho_{SD_f}\right)\gamma_S+H_{ff}\gamma_{U_f}+H_{nf}\gamma_{U_n}+1}<\gamma_{\text{thf}}^{\text{DL}}\right)\\ &= \Pr\left(\rho_{SD_f}<V_1\rho_{ff}+V_2\rho_{nf}+V_3\right)\\ &= \int_0^\infty f_{\rho_{ff}}(z)\int_0^\infty f_{\rho_{nf}}(y)\int_0^{V_1z+V_2y+V_3} f_{\rho_{SD_f}}(x)dxdydz. \quad \text{(A.1)}\end{aligned}$$

By using the PDF and CDF of ρ_i, (A.1) can be further expressed as

$$\mathrm{P}_{\text{out,nid}}^{D_f}=\int_0^\infty\frac{1}{\beta_{ff}}e^{-\frac{z}{\beta_{ff}}}\int_0^\infty\frac{1}{\beta_{nf}}e^{-\frac{y}{\beta_{nf}}}\left(1-e^{-\frac{V_1z+V_2y+V_3}{\beta_{SD_f}}}\right)dydz. \quad \text{(A.2)}$$

Then, we can obtain (10) after some routine mathematical manipulations.

Appendix B: Proof of Theorem 2

Similar to Theorem 1, upon substituting (5) and (6) into (15), after some mathematical manipulations, the OP of D_f can be rewritten as

$$\begin{aligned}\mathrm{P}_{\text{out,nid}}^{D_n} &= \Pr\left(\rho_{SD_n}<W_1\rho_{fn}+W_2\rho_{nn}+W_3\right)\\ &= \int_0^\infty f_{\rho_{fn}}(z)\int_0^\infty f_{\rho_{nn}}(y)\int_0^{W_1z+W_2y+W_3} f_{\rho_{SD_n}}(x)dxdydz. \quad \text{(B.1)}\end{aligned}$$

By using the PDF and CDF of ρ_i, (B.1) can be further expressed as

$$\mathrm{P}_{\text{out,nid}}^{D_n}=\int_0^\infty\frac{1}{\beta_{fn}}e^{-\frac{z}{\beta_{fn}}}\int_0^\infty\frac{1}{\beta_{nn}}e^{-\frac{y}{\beta_{nn}}}\left(1-e^{-\frac{W_1z+W_2y+W_3}{\beta_{SD_n}}}\right)dydz. \quad \text{(B.2)}$$

Then, we can obtain (16) after some basic mathematical manipulations.

Appendix C: Proof of Theorem 3

Upon substituting (8) into (19), as well as carrying out some basic mathematical manipulations, the OP of U_n can be rewritten as

$$\begin{aligned}\mathrm{P}_{\text{out,nid}}^{U_n} &= \Pr\left(\rho_{SU_n}<A_1\rho_{SU_f}+A_2\rho_{LI}+A_3\rho_{SS}+A_4\right)\\ &= \int_0^{A_1x+A_2y+A_3z+A_4} f_{\rho_{SU_n}}(w)\int_0^\infty f_{\rho_{SU_f}}(x)\\ &\quad\times\int_0^\infty f_{\rho_{LI}}(y)\int_0^\infty f_{\rho_{SS}}(z)dwdxdydz. \quad \text{(C.1)}\end{aligned}$$

From (C.1), it can be inferred that the PDF and CDF of ρ_{SU_n}, ρ_{SU_f}, and ρ_{LI} are all established, but these of ρ_{SS} are still to be developed for the bidirectional sensing channels. To this end, we derive the PDF and CDF of ρ_{SS} in the following.

Since the signals are broadcast at the speed of light through the atmosphere, we assume that $h_{ST}=h_{TS}$. By using the CDF of ρ_{ST} and ρ_{TS}, we can further obtain

$$\begin{aligned}F_{\rho_{SS}}(z) &= \Pr\left(\rho_{SS}=\rho_{ST}^2=\rho_{TS}^2\leqslant z\right)\\ &= \int_0^{\sqrt{z}} f_{\rho_{ST}}(t)dt=\int_0^{\sqrt{z}} f_{\rho_{TS}}(t)dt\\ &= 1-e^{-\frac{\sqrt{z}}{\beta_{ST}}}=1-e^{-\frac{\sqrt{z}}{\beta_{TS}}}. \quad \text{(C.2)}\end{aligned}$$

By using the variable substitution technique, and taking the first derivative of $F_{\rho_{SS}}(z)$ with respect to z, the PDF of ρ_{SS} is given by

$$f_{\rho_{SS}}(z)=\frac{1}{2\beta_{SS}\sqrt{z}}e^{-\frac{\sqrt{z}}{\beta_{SS}}}. \quad \text{(C.3)}$$

Upon substituting the PDF of ρ_i and (C.3) into (C.1), the OP of U_n can be further expressed as

$$\begin{aligned}\mathrm{P}_{\text{out,nid}}^{U_n} &= \int_0^\infty\frac{1}{\beta_{LI}}e^{-\frac{y}{\beta_{LI}}}\int_0^\infty\frac{1}{2\beta_{SS}\sqrt{z}}e^{-\frac{\sqrt{z}}{\beta_{SS}}}\\ &\quad\times\int_0^\infty\frac{1}{\beta_{SU_f}}e^{-\frac{x}{\beta_{SU_f}}}\left(1-e^{-\frac{A_1x+A_2y+A_3z+A_4}{\beta_{SU_n}}}\right)dxdydz. \quad \text{(C.4)}\end{aligned}$$

Finally, with the aid of [51, Eq. (3.322.2)], (20) can be obtained after some further mathematical manipulations.

Appendix D: Proof of Theorem 4

Upon substituting (8) and (9) into (15), after some basic mathematical manipulations, the OP of U_f can be rewritten as

$$\begin{aligned}\mathrm{P}_{\text{out,nid}}^{U_f} &= 1-\Pr\left(A_1\rho_{SU_f}+A_2\rho_{LI}+A_3\rho_{SS}+A_4<\rho_{SU_n}\right.\\ &\qquad\left.<B_1\rho_{SU_f}-B_2\rho_{LI}-B_3\rho_{SS}-B_4\right)\\ &= 1-\int_{A_1x+A_2y+A_3z+A_4}^{B_1x-B_2y-B_3z-B_4} f_{\rho_{SU_n}}(w)\int_0^\infty f_{\rho_{SU_f}}(x)\\ &\quad\times\int_0^\infty f_{\rho_{LI}}(y)\int_0^\infty f_{\rho_{SS}}(z)dwdxdydz. \quad \text{(D.1)}\end{aligned}$$

Upon substituting the PDF of ρ_i and (C.3) into (D.1), the OP of U_f can be further expressed as

$$\begin{aligned}\mathrm{P}_{\text{out,nid}}^{U_f} &= 1-\int_0^\infty\frac{1}{\beta_{LI}}e^{-\frac{y}{\beta_{LI}}}\int_0^\infty\frac{1}{2\beta_{SS}\sqrt{z}}e^{-\frac{\sqrt{z}}{\beta_{SS}}}\int_0^\infty\frac{1}{\beta_{SU_f}}\\ &\quad\times e^{-\frac{x}{\beta_{SU_f}}}\left(e^{-\frac{A_1x+A_2y+A_3z+A_4}{\beta_{SU_n}}}-e^{-\frac{B_1x-B_2y-B_3z-B_4}{\beta_{SU_n}}}\right)dxdydz. \quad \text{(D.2)}\end{aligned}$$

Finally, with the aid of [51, Eq. (3.322.2)], we can obtain (25) after some routine mathematical manipulations.

REFERENCES

[1] X. You, C. Wang, J. Huang, and et al., "Towards 6G wireless communication networks:vision, enabling technologies, and new paradigm shifts," *Sci. China Inf. Sci.*, vol. 64, no. 1, pp. 1–74, Dec. 2021.

[2] F. Liu, Y. Cui, C. Masouros, J. Xu, T. X. Han, Y. C. Eldar, and S. Buzzi, "Integrated sensing and communications: Toward dual-functional wireless networks for 6G and beyond," *IEEE J. Sel. Areas Commun.*, vol. 40, no. 6, pp. 1728–1767, Jun. 2022.

[3] D. C. Nguyen, M. Ding, P. N. Pathirana, A. Seneviratne, J. Li, D. Niyato, O. Dobre, and H. V. Poor, "6G Internet of Things: A comprehensive survey," *IEEE Internet Things J.*, vol. 9, no. 1, pp. 359–383, Jan. 2022.

[4] F. Liu, C. Masouros, A. Li, H. Sun, and L. Hanzo, "MU-MIMO communications with MIMO radar: From co-existence to joint transmission," *IEEE Trans. Wireless Commun.*, vol. 17, no. 4, pp. 2755–2770, Apr. 2018.

[5] F. Liu, C. Masouros, A. P. Petropulu, H. Griffiths, and L. Hanzo, "Joint radar and communication design: Applications, state-of-the-art, and the road ahead," *IEEE Trans. Commun.*, vol. 68, no. 6, pp. 3834–3862, Jun. 2020.

[6] F. Wang and H. Li, "Power allocation for coexisting multicarrier radar and communication systems in cluttered environments," *IEEE Trans. Signal Process.*, vol. 69, pp. 1603–1613, Feb. 2021.

[7] J. Yang, C.-K. Wen, and S. Jin, "Hybrid active and passive sensing for SLAM in wireless communication systems," *IEEE J. Sel. Areas Commun.*, pp. 1–18, Mar. 2022.

[8] H. Tataria, M. Shafi, A. F. Molisch, M. Dohler, H. Sjöland, and F. Tufvesson, "6G wireless systems: Vision, requirements, challenges, insights, and opportunities," *Proc. IEEE*, vol. 109, no. 7, pp. 1166–1199, Jul. 2021.

[9] Y. Liu, Z. Qin, M. Elkashlan, Z. Ding, A. Nallanathan, and L. Hanzo, "Non-orthogonal multiple access for 5G and beyond," *Proc. IEEE*, vol. 105, no. 12, pp. 2347–2381, Dec. 2017.

[10] C.-X. Wang, X. You, X. Gao, and et al., "On the road to 6G: Visions, requirements, key technologies and testbeds," *IEEE Commun. Surveys & Tutorials*, pp. 1–71, Early Access 2023.

[11] M. Vaezi, A. Azari, S. R. Khosravirad, M. Shirvanimoghaddam, M. M. Azari, D. Chasaki, and P. Popovski, "Cellular, wide-area, and non-terrestrial IoT: A survey on 5G advances and the road toward 6G," *IEEE Commun. Surveys & Tutorials*, vol. 24, no. 2, pp. 1117–1174, Secondquarter 2022.

[12] X. Mu, Z. Wang, and Y. Liu, "NOMA for integrating sensing and communications towards 6G: A multiple access perspective," *IEEE Wireless Commun.*, pp. 1–8, Early Access 2023.

[13] H. Li, J. Li, M. Liu, Z. Ding, and F. Gong, "Energy harvesting and resource allocation for cache-enabled UAV based IoT NOMA networks," *IEEE Trans. Veh. Technol.*, vol. 70, no. 9, pp. 9625–9630, Sept. 2021.

[14] Z. Wang, Y. Liu, X. Mu, and Z. Ding, "NOMA inspired interference cancellation for integrated sensing and communication," in *ICC 2022 - IEEE International Conf. Commun.*, Aug. 2022, pp. 3154–3159.

[15] C. Zhang, W. Yi, and Y. Liu, "Semi-integrated-sensing-and-communication (Semi-ISaC) networks assisted by NOMA," in *ICC 2022 - IEEE International Conf. Commun.*, Aug. 2022.

[16] X. Mu, Y. Liu, L. Guo, J. Lin, and L. Hanzo, "NOMA-aided joint radar and multicast-unicast communication systems," *IEEE J. Sel. Areas Commun.*, vol. 40, no. 6, pp. 1978–1992, Mar. 2022.

[17] Z. Wang, Y. Liu, X. Mu, Z. Ding, and O. A. Dobre, "NOMA empowered integrated sensing and communication," *IEEE Commun. Lett.*, vol. 26, no. 3, pp. 677–681, Mar. 2022.

[18] C. Ouyang, Y. Liu, and H. Yang, "On the performance of uplink ISAC systems," *IEEE Commun. Lett.*, vol. 26, no. 8, pp. 1769–1773, Aug. 2022.

[19] ——, "Revealing the impact of SIC in NOMA-ISAC," *IEEE Wireless Commun. Lett.*, pp. 1–5, 2023.

[20] M. Rihan and L. Huang, "Non-orthogonal multiple access based cooperative spectrum sharing between MIMO radar and MIMO communication systems," *Digit. Signal Process.*, vol. 83, pp. 107–117, Dec. 2018.

[21] M. Liu, M. Yang, H. Li, K. Zeng, Z. Zhang, A. Nallanathan, G. Wang, and L. Hanzo, "Performance analysis and power allocation for cooperative ISAC networks," *IEEE Internet Things J.*, vol. 10, no. 7, pp. 6336–6351, Apr. 2023.

[22] Z. Yang, D. Li, N. Zhao, Z. Wu, Y. Li, and D. Niyato, "Secure precoding optimization for NOMA-aided integrated sensing and communication," *IEEE Trans. Commun.*, vol. 70, no. 12, pp. 8370–8382, Dec. 2022.

[23] E. Björnson, M. Matthaiou, and M. Debbah, "A new look at dual-hop relaying: Performance limits with hardware impairments," *IEEE Trans. Commun.*, vol. 61, no. 11, pp. 4512–4525, Nov. 2013.

[24] C. K. Singh and P. K. Upadhyay, "Overlay cognitive IoT-based full-duplex relaying NOMA systems with hardware imperfections," *IEEE Internet Things J.*, vol. 9, no. 9, pp. 6578–6596, May 2022.

[25] O. Ozdemir, R. Hamila, and N. Al-Dhahir, "I/Q imbalance in multiple beamforming OFDM transceivers: SINR analysis and digital baseband compensation," *IEEE Trans. Commun.*, vol. 61, no. 5, pp. 1914–1925, May 2013.

[26] X. Li, Q. Wang, M. Liu, J. Li, H. Peng, M. J. Piran, and L. Li, "Cooperative wireless-powered NOMA relaying for B5G IoT networks with hardware impairments and channel estimation errors," *IEEE Internet Things J.*, vol. 8, no. 7, pp. 5453–5467, Apr. 2021.

[27] S. Biswas, K. Singh, O. Taghizadeh, and T. Ratnarajah, "Coexistence of MIMO radar and FD MIMO cellular systems with QoS considerations," *IEEE Trans. Wireless Commun.*, vol. 17, no. 11, pp. 7281–7294, Nov. 2018.

[28] ——, "Design and analysis of FD MIMO cellular systems in coexistence with MIMO radar," *IEEE Trans. Wireless Commun.*, vol. 19, no. 7, pp. 4727–4743, Jul. 2020.

[29] L. Chen, F. Liu, W. Wang, and C. Masouros, "Joint radar-communication transmission: A generalized Pareto optimization framework," *IEEE Trans. Signal Process.*, vol. 69, pp. 2752–2765, May 2021.

[30] K. Guo, K. An, F. Zhou, T. A. Tsiftsis, G. Zheng, and S. Chatzinotas, "On the secrecy performance of NOMA-based integrated satellite multiple-terrestrial relay networks with hardware impairments," *IEEE Trans. Veh. Technol.*, vol. 70, no. 4, pp. 3661–3676, Apr. 2021.

[31] P. Liu and T. Jiang, "Channel estimation performance analysis of massive MIMO IoT systems with Ricean fading," *IEEE Internet Things J.*, vol. 8, no. 7, pp. 6114–6126, Apr. 2021.

[32] M. H. Al-Ali and K. C. Ho, "Transmit precoding in underlay MIMO cognitive radio with unavailable or imperfect knowledge of primary interference channel," *IEEE Trans. Wireless Commun.*, vol. 15, no. 8, pp. 5143–5155, Aug. 2016.

[33] N. Su, F. Liu, and C. Masouros, "Secure radar-communication systems with malicious targets: Integrating radar, communications and jamming functionalities," *IEEE Trans. Wireless Commun.*, vol. 20, no. 1, pp. 83–95, Jan. 2021.

[34] N. Su, F. Liu, Z. Wei, Y.-F. Liu, and C. Masouros, "Secure dual-functional radar-communication transmission: Exploiting interference for resilience against target eavesdropping," *IEEE Trans. Wireless Commun.*, vol. 21, no. 9, pp. 7238–7252, Sept. 2022.

[35] Y. Sun, D. W. K. Ng, J. Zhu, and R. Schober, "Robust and secure resource allocation for full-duplex MISO multicarrier NOMA systems," *IEEE Trans. Commun.*, vol. 66, no. 9, pp. 4119–4137, Sept. 2018.

[36] S. Guo and X. Zhou, "Robust resource allocation with imperfect channel estimation in NOMA-based heterogeneous vehicular networks," *IEEE Trans. Commun.*, vol. 67, no. 3, pp. 2321–2332, Mar. 2019.

[37] X. Li, M. Liu, C. Deng, P. T. Mathiopoulos, Z. Ding, and Y. Liu, "Full-duplex cooperative NOMA relaying systems with I/Q imbalance and imperfect SIC," *IEEE Wireless Commun. Lett.*, vol. 9, no. 1, pp. 17–20, Jan. 2020.

[38] M. Li, F. E. Bouanani, L. Tian, W. Chen, Z. Han, and S. Muhaidat, "Error rate analysis of non-orthogonal multiple access with residual hardware impairments," *IEEE Commun. Lett.*, vol. 25, no. 8, pp. 2522–2526, Aug. 2021.

[39] N. P. Le, L. C. Tran, X. Huang, J. Choi, E. Dutkiewicz, S. L. Phung, and A. Bouzerdoum, "Performance analysis of uplink NOMA systems with hardware impairments and delay constraints over composite fading channels," *IEEE Trans. Veh. Technol.*, vol. 70, no. 7, pp. 6881–6897, Jul. 2021.

[40] X. Li, J. Li, Y. Liu, Z. Ding, and A. Nallanathan, "Residual transceiver hardware impairments on cooperative NOMA networks," *IEEE Trans. Wireless Commun.*, vol. 19, no. 1, pp. 680–695, Jan. 2020.

[41] X. Yue, Y. Liu, S. Kang, A. Nallanathan, and Z. Ding, "Spatially random relay selection for full/half-duplex cooperative NOMA networks," *IEEE Trans. Commun.*, vol. 66, no. 8, pp. 3294–3308, Aug. 2018.

[42] M. Richards, *Fundamentals of Radar Signal Processing*. New York, NY, USA: McGraw-Hill Education, 2014.

[43] Z. Zhang, H. Sun, and R. Q. Hu, "Downlink and uplink non-orthogonal multiple access in a dense wireless network," *IEEE J. Sel. Areas Commun.*, vol. 35, no. 12, pp. 2771–2784, Dec. 2017.

[44] H. Zeng, X. Zhu, Y. Jiang, Z. Wei, S. Sun, and X. Xiong, "Toward UL-DL rate balancing: Joint resource allocation and hybrid-mode multiple access for UAV-BS-Assisted communication systems," *IEEE Trans. Commun.*, vol. 70, no. 4, pp. 2757–2771, Apr. 2022.

[45] Z. Zhang, B. Chen, and M. Yang, "Moving target detection based on time reversal in a multipath environment," *IEEE Trans. Aerosp. Electron. Syst.*, vol. 57, no. 5, pp. 3221–3236, Oct. 2021.

[46] M. A. Richards, J. A. Sheer, and W. A. Holm, *Principles of Modern Radar: Basic Principles*. Raleigh, North Carolina: SciTech Publishing, 2010.

[47] D. W. Bliss and S. Govindasamy, *Adaptive Wireless Communications: MIMO Channels and Networks.* New York, NY, USA: Cambridge University Press, 2013.

[48] W. Duan, Y. Ji, J. Hou, B. Zhuo, M. Wen, and G. Zhang, "Partial-DF full-duplex D2D-NOMA systems for IoT with/without an eavesdropper," *IEEE Internet Things J.*, vol. 8, no. 8, pp. 6154–6166, Apr. 2021.

[49] Z. Luo, W. Ma, A. M. So, Y. Ye, and S. Zhang, "Semidefinite relaxation of quadratic optimization problems," *IEEE Signal Process. Mag.*, vol. 27, no. 3, pp. 20–34, May 2010.

[50] J. Men, J. Ge, and C. Zhang, "Performance analysis of nonorthogonal multiple access for relaying networks over Nakagami-m fading channels," *IEEE Trans. Veh. Technol.*, vol. 66, no. 2, pp. 1200–1208, Feb. 2017.

[51] I. S. Gradshteyn and I. M. Ryzhik, *Table of Integrals, Series, and Products, 7th ed.* New York, NY, USA: Academic, 2007.